Hydrogen Diffusion in Amorphous $Ni_{60}Zr_{40}$

Yi Zhao

Dept. Physics, McGill Univ., 3600 Univ. st.
Montréal, Québec, Canada, H3A 2T8.

February 18, 1991

Abstract

Electrochemical methods have been used to measure the solubility and diffusivity of hydrogen in amorphous $Ni_{60}Zr_{40}$ over a wide range of hydrogen concentrations . It is found that Sievert's law is not obeyed and that the concentration of hydrogen in the metallic glass varies as $P^{1/4}$, P being the pressure of hydrogen. In the concentration range of hydrogen measured, the diffusion constant of hydrogen increases by more than a factor of ten. A Gaussian distribution of hydrogen binding energy was used to explain the concentration dependence of chemical potential. A possible explanation to the concentration dependence of diffusion coefficient was also given.

Résumé

Des méthodes électrochimiques ont été utilisées pour mesurer la solubilité et la diffusivité de l' hydrogène dans des échantillons amorphes de $Ni_{60}Zr_{40}$ sur un large domaine de concentration en hydrogène. Les résultats ont révélé que la loi de Sievert n'est pas respectèe mais que la concentration d'hydrogène dans le métal amorphe varie comme $P^{1/4}$; P étant la pression d'hydrogène. Dans le domaine de concentration mesurée pour l'hydrogène, la constante de diffusion de l'hydrogène augmente d'un facteur supérieur à 10. Une distribution gaussienne de l'énergie de liaison de l'hydrogène a été utilisée pour restiture la dépendance du potentiel chimique avec la concentration. Une explication est proposée pour exprimer la variation du coefficient de diffusion avec la concentration.

Contents

List of Figures

List of Tables

Acknowledgment

This work was supported by the Minstere de L'Energie et des Ressources of the Province of Quebec, Canada.

Prof. John O. Ström-Olsen and Prof. Dominic H. Ryan first suggested that I investigate the diffusion behavior of hydrogen by electrochemical method During the project, they gave me continuous advise and support. With this opportunity, I'd like to give them the special thanks. Mr. Huai Yiming and Prof. Robert W Cochrane helped me in making the samples, Mr. Andrew Dawson helped me in computer programming Dr. Michel Trudeau measured the composition of the sample, Mr Frank Van Gils helped me a lot in technical problem, Mr. Liao Lexiang give me lots of advice in using the melt-spinning machine. Without those kindly help, few progress can be made quickly.

Finally, I'd like to thank professors and students in physics department for their pleasant cooperation during this project. Working with them is always a pleasure

Chapter 1

Introduction

In 1866, Thomas Graham[1] discovered that Pd absorbs large amount of hydrogen gas which also diffused through the metal several orders of magnitude faster than other gases He suggested that Pd could be used either to extract hydrogen from a gas stream or to purify it. Since then, the field of metal hydrides has continued to attract the interest of scientists. In addition to various possible applications(e.g the potential of metal hydrides to moderate nuclear reactors and to store hydrogen reversibly), physicists were interested in the fact that metal-hydrogen systems exhibit many key phenomena of solid state physics such as magnetism and superconductivity : heavy electron behavior; alloy formation; superlattices[2]; fractal behavior; metal- semiconductor transitions in the bulk and at the surface; surface reconstruction and surface segregation; phase diagrams; order-disorder transitions; quantum diffusion; formation of disordered and non-crystalline materials.

Two quantities, the solubility and diffusivity in metal hydrides, are important for many applications. For example for hydrogen storage, solubility directly determines the amount of hydrogen that can be stored , while diffusivity will determine the kinetics of loading or extracting hydrogen.

A great amount of data exists for both crystalline and amorphous metal hydrides systems. In crystalline materials, there is usually a phase transition at high hydrogen concentrations[3]. This appears, as a plateau in the pressure-concentration (p-c) isotherms, which is helpful for hydrogen storage since a large increase of hydrogen concentration can be effected with little increase in hydrogen pressure. The diffusion of hydrogen in crystalline metal hydrides usually obeys an Arrhenius law implying that there is a well-defined activation energy for the hydrogen diffusion process. However in amorphous metals no plateau has yet been found in p-c isotherms and non-Arrhenius behavior for the diffusion is also found (see fig.1.1 for the comparison of p-c isotherms of crystalline and amorphous metal hydrides.).

The absorption of large amounts of hydrogen usually causes the metal lattice to expand and makes an alloy or metal brittle. For crystalline metals or intermetallic compounds, the embrittlement together with the expansion will pulverize the metal after a few cycles of hydrogenation. For amorphous alloys, however, the material can keep its shape even after many cycles of absorption and desorption of hydrogen. The ductility of the material can be recovered after the hydrogen is driven out the material. This property of amorphous alloys, therefore, makes the material easier to handle when used as a hydrogen storage media. It may seem that the nonexistence of plateau in p-c isotherms does not favor the use of amorphous metal-hydrogen system

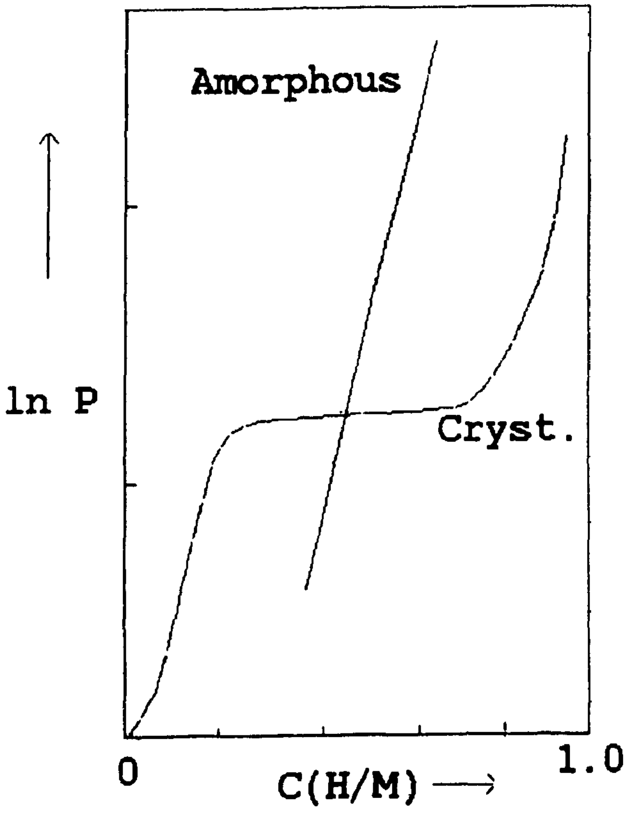

Figure 1.1: Schematic diagram of p-c isotherms of crystalline and amorphous materials

as hydrogen storage medium. However, a sufficiently low slope[17] to give a reasonable change in storage for a change in pressure, together with good kinetics, would make the material usable. Furthermore, some amorphous alloys have larger total absorption than their crystalline counterparts. For these reasons it is worth looking at high hydrogen-absorbing amorphous alloys.

There are many ways to study p-c isotherms and hydrogen diffusion. The sample may be charged with hydrogen directly from the gas phase, or electrolytically, or even by proton implantation. The diffusion coefficient can be measured by NMR, from the absorption and desorption rate[4], by electrochemical methods[5], or by mechanical relaxation[6]. But compared other methods, the electrochemical method, which we mainly used in this study and will be detail described in Chapter 3 , has the following advantages:

- It can measure small changes in chemical potential precisely, measurements that in gas loading require sensing extremely small pressure changes.
- It can measure the chemical potential and diffusion coefficient simultaneously.
- It eliminates the dissociation process of hydrogen at the metal surface. (In gas charging, hydrogen molecules have to dissociate at the metal surface into hydrogen atoms in order to get into the metal. In electrochemical method , hydrogen exists in the electrolyte in the form of H^+, it will give out its charge at the metal surface to become atomic hydrogen, and then goes into the metals, so facilitating the charging process.)

The only drawback of the electrochemical method is that it may increase the possibility of contamination at the interface between electrolyte and the metal. This problem can, to some extent, be solved by treatment of the sample[7](e.g. polishing with emery paper).

This method was therefore chosen to do the measurements in this thesis. It is actually a double cell technique[7]. Each cell is equipped with a reference electrode, which has constant chemical potential and is made from calomel(Hg_2Cl_2), saturated KCl, Hg and Pt wire (The electrode is called a saturated calomel electrode), and a counter electrode which is a Pt sheet and is used for passing and counting the large current when charging the sample with hydrogen. The sample is then used as a common grounded electrode for both cells. At rest, both sides are open circuit and the potential difference between each face of the sample and the corresponding reference electrode is measured. Loading the sample with hydrogen is done by applying a current pulse at one cell (the entry side for hydrogen), which creates *H* at one surface of the sample and so changes the potential difference at this side instantaneously. After the pulse (the system being now in the rest condition), the chemical potential or the potential difference at this side will decay, whereas at the other side (the exit side), after a short delay, the chemical potential will arise as the hydrogen diffuses through. Fitting the transient at the exit side with a solution for the diffusion equation at this boundary condition (current-pulse charging and open circuit afterwards), we can obtain the diffusion coefficient. At the same time, when the transient becomes saturated, we can also obtain the equilibrium chemical potential. Fig.1.2 is a schematic diagram of such chemical potential change at both sides after the current pulse was applied.

In Chapter 2, amorphous metal-hydrogen systems are reviewed. Then the details of measurement principles and experimental set-up are given in Chapter 3. Chapter 4, gives the results and discussions and Chapter 5 presents the conclusions.

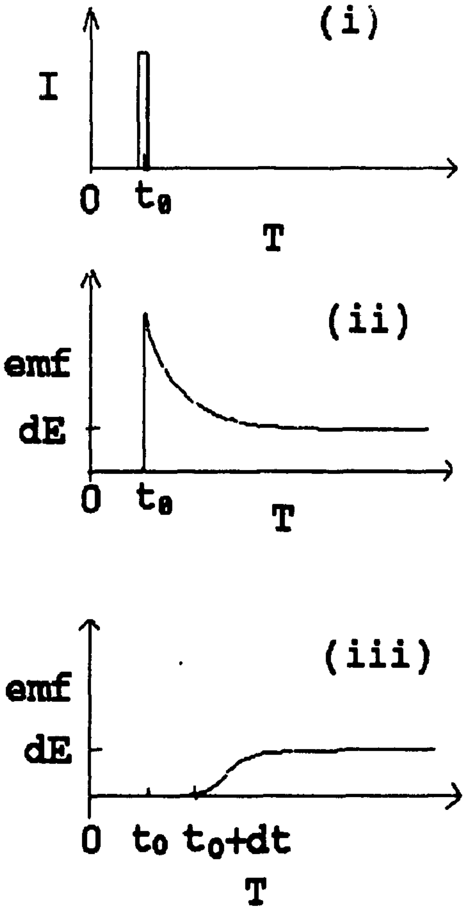

Figure 1.2: Schematic diagram of emf changes in current pulse technique. (i) A current pulse applied at t_0; (ii) The emf changes at the entry side; (iii) The emf changes at the exit side

Chapter 2

Hydrogen in amorphous metals

This review will be confined to those properties which relate to the title of this thesis, namely the site occupancy, solubility and diffusivity. A comparison between amorphous and crystalline metal hydrides is given whenever possible.

2.1 Site occupancy

Because of the disordered structure of amorphous alloys, it is difficult to determine uniquely the nature of the sites occupied by hydrogen. There exists, however, considerable evidence that hydrogen occupancy in many amorphous hydrides consists of a series of sites with a quasi- continuous range of energies.

In 1980, J.J.Rush et al., from inelastic neutron scattering data in amorphous $TiCuH_{1.3}$[11], found, from the neutron intensity versus energy transfer, the same peak position at the spectrum as for crystalline $TiCuH_{0.93}$, but that the width of the spec-

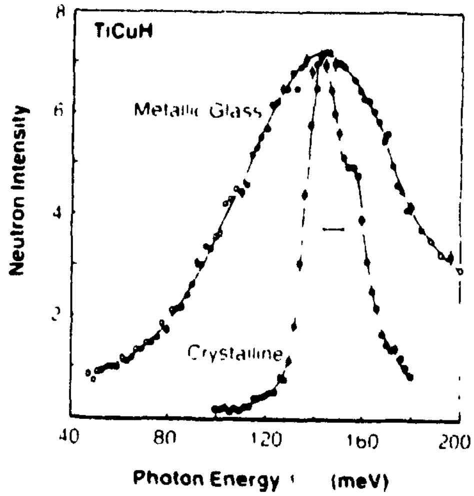

Figure 2.1: Neutron inelastic scattering spectra measured at 78K for crystalline $TiCuH_{0.93}$ and for amorphous $TiCuH_{1.3}$(from ref.[2]). The energy resolution (FWHM) near the peak is indicated by the horizontal bar

trum was approximately 4 times wider in the amorphous than in the crystalline alloy(see Fig.2.1). They interpreted this as indicative of a wide distribution of local environments for hydrogen.

H. Kaneko and co-workers reported a similar result for amorphous Ni-Zr [12] by comparing the neutron inelastic scattering spectra of amorphous $NiZrH_{1.8}$ with the crystalline hydride $NiZrH_{2.8}$. Both spectra had pronounced peaks at approximately 120meV representing the primary vibration mode of the solute hydrogen, but the peak width associated with the amorphous sample was about twice as wide as the crystalline material. However, whereas Rush and coworkers observed a single, broad, symmetric peak in their scattering spectra for amorphous Cu-Ti hydrides, Kaneko and coworkers found a number of (overlapping) peaks in their measurement. They assigned the central, high intensity peak to hydrogen vibration in a site tetrahedrally coordinated to metal atoms (similar to the so-called c-site in the crystalline NiZr hydride) and a smaller, secondary peak as representing H vibration in a hexhydral(six-fold coordinated) site (similar to the b-site in the NiZr hydride crystal). In fact, by assuming that the ratio of tetrahedra to hexhydra was the same as the crystal (about 2), they proposed a statistical model for hydrogen sites in amorphous alloys with a view to explaining trends in hydrogen capacity as a function of alloy composition.

In 1981, K.Kai et al. [13] used X-ray diffraction and pulsed neutron total scattering measurements to construct the structure factor S(Q) for amorphous $Pd_{35}Zr_{65}$ melt-quenched ribbons loaded with hydrogen ($Pd_{35}Zr_{65}H_{101}$) or deuterium($Pd_{35}Zr_{65}D_x$ x=0, 17, 42, 85, 125) (see Fig.2.2) By Fourier transforming the X-ray derived S(Q) for the hydrogenated sample, these workers constructed the pair correlation function g(r) and the radial distribution function(RDF) given by $4\pi r^2 \rho g(r)$. Kai et al. found that the first peak in the RDF of the unhydrogenated sample split into two distinct sub-peaks at the $Pd_{35}Zr_{65}H_{101}$ composition. This splitting was interpreted as a hydrogen-induced expansion of the Zr-Zr nearest-neighbor distance(from 3.20A to 3.32A) while the Pd-Pd and Pd-Zr distances were left unchanged. They found a similar effect in the RDF derived from neutron scattering on the $Pd_{35}Zr_{65}D_x$ alloys Additionally, they fitted this spectra with a superposition of two gaussian peaks, and determined the coordination number of metal atoms around the H or D by the area under these peaks. They found that the coordination number changes with H or D concentration. At low hydrogen or deuterium loadings, H or D is located in distorted tetrahedral sites comprised of 4 Zr atoms. At higher H or D concentrations, they suggest that D or H occupies octahedral sites in the amorphous structure. At still higher concentrations($H/M = 1.25$), they

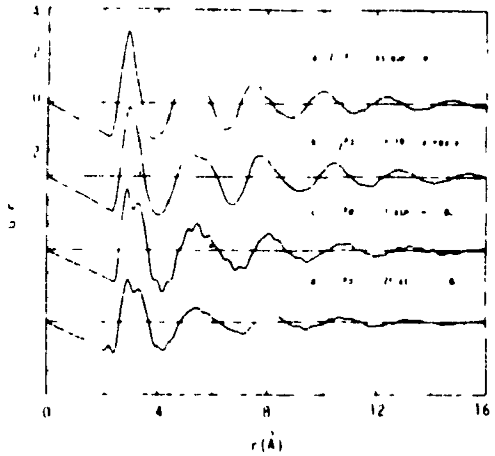

Figure 2.2: The reduced radial distribution functions G(r) obtained for (a) Zr_2Pd as quenched (b) Zr_2Pd annealed at 190C for 11 hrs (c) $Zr_2PdH_{2.7}$ and (d) $Zr_2PdH_{3.0}$ (from ref.[8])

concluded that the average local atomic arrangement of 5 metal atoms around a H atom previals(hexhydral sites).

Suzuki et al.[14] described the results of inelastic neutron and neutron total scattering experiments utilizing short wavelength pulsed neutrons, used to probe the local H environment in amorphous NiZr melt quenched ribbons Similar to Kai, they obtained the coordination number changing with deuterium concentration. For low H loadings, they found that H occupies an interstitial hole surrounded by 4 Zr atoms The coordinating number of Zr changes from 4 to 3, while the coordinating number of Ni changes from 0 to 1 when the concentration of H was raised They concluded that at low concentrations, H occupies the interstitial hole surrounded by 4 Zr atoms, and at higher concentrations, sites surrounded by 3 Zr and 1 Ni atoms begin to be filled.

Similar findings were given by Samwer and Johnson [15] from a X-Ray scattering experiments on Pd-Zr and Rh-Zr melt-quenched ribbons

Mossbauer spectroscopy measurement have also yield information even though they do not directly reflect hydrogen characteristics but are only sensitive to changes in the host atom environment. As S.M. Fries et al.[16] illustrate, sensitivity to the Fe nearest neighbors in the metallic glass system Fe-Zr can be used to infer the hydrogen occupation characteristics of that material [16]. They found that at low H content, the Fe environment is relatively undisturbed beyond effects due to lattice expansion: at higher H levels, Fe is more directly affected when H/Zr exceeds 2.

2.2 Solubility

There are several ways to charge a metal with hydrogen. Here we focus on the two common methods, namely electrochemically and from the gas phase.

In charging from the gas phase, the amorphous metal is exposed to hydrogen gas at a fixed temperature. After H_2 dissociates at the surface, H atoms may diffuse into the bulk alloy. This process proceeds until the chemical potential of hydrogen in the metal μ_H is equal to that in the gas phase μ^G. After equilibrium is attained, μ_H can be calculated by measuring the final equilibrium gas pressure P, assuming ideal gas behavior, using simple thermodynamics

$$\mu_H = \mu^G = RTlnP - TS_o \tag{2.1}$$

where T is the temperature, S_o the standard entropy of H_2 gas, and here the chemical potential is expressed per mole of H_2 in both the gas and the metal. The amount of hydrogen absorbed by the sample can be determined by measuring weight changes with a fine quartz spring or by volumetric techniques. The p-c isotherm is deduced by performing this measurement over a range of external pressures at fixed T and relating each particular value of pressure (or chemical potential) to the total amount of hydrogen absorbed under that pressure.

Gas phase absorption isotherms have been measured for $Ni-Zr$[17, 21, 20], $Cu-Ti$[24, 22],$Cu-Zr$[23],and $Fe-Ti$ [24]. Up to now, no plateau has been found in the p-c isotherms.

The first work for amorphous Ni-Zr was done by Spit et al. [21] for $Ni_{64}Zr_{36}$ (They also investigated amorphous $Ni_{62}Ti_{29}Zr_9$.) Sievert's law, which relates the concentration of hydrogen to the square root of the hydrogen pressure(usually valid when H concentration is small and occupy one type of site with a single binding energy), was not obeyed. No plateau was observed for the p-c isotherm of amorphous samples, even through a plateau was observed for all corresponding crystalline alloys. The maximum absorption is typically one third smaller than in the crystalline counterpart under the same conditions of temperature and pressure. The ribbons remained amorphous upon absorption and desorption, as shown by X-ray diffraction. Upon hydrogen absorption the amorphous ribbons typically increased with about 3.5% in length and width. The ribbons became brittle but did not break up, in contrast to crystalline alloys

In 1986, Batalla et al. [17] carefully measured p-c isotherms (see fig.2.3) of a wide variety of amorphous NiZr alloys by gas charging at a range of temperatures and pressures. By combining the results of the p-c isotherms with a careful study of the thermodynamics of desorption by scanning calorimetry, they got further support for the picture of a spread in binding energy for hydrogen sites. Again, no phase separation

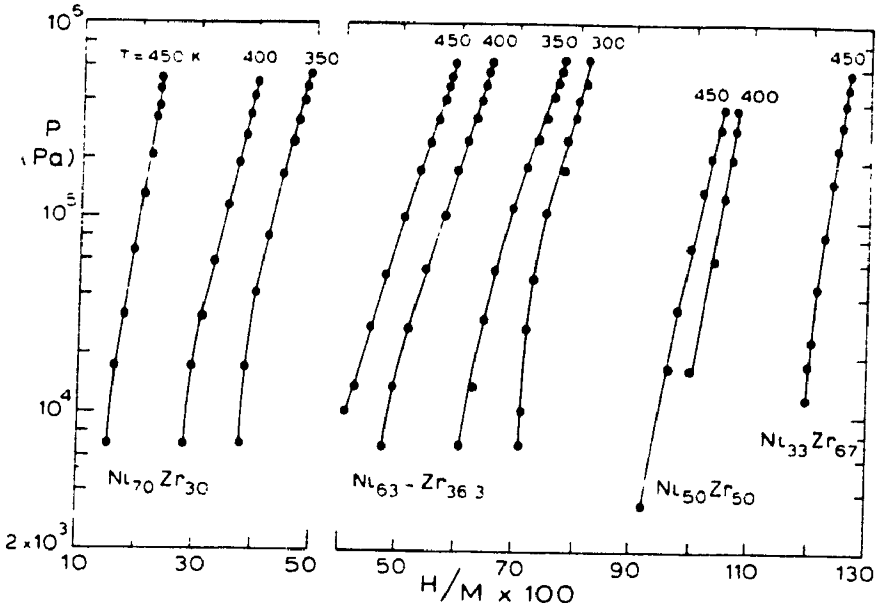

Figure 2.3: Pressure-composition isotherms for amorphous Ni-Zr alloys at various temperatures.(from ref.[17])

was found by X-ray powder diffraction. They complemented the measurements with a calculation of hydrogen site-binding energies using the embedded atom model[18]. and site-statistics of Ni-Zr using a computer-generated amorphous cluster. Hydrogen site statistics were determined by generating a dense random packed cluster of 1000 hard spheres using the Bennett[19] algorithm with a fraction x of spheres labeled as Zr. Lennard-Jones potentials were imposed and adjusted until the partial structure factors agreed with experimental values. Then they used the effective medium approximation developed by Norskov and Lang[33] to calculate the hydrogen binding energies for the specific configurations of distorted tetrahedral sites found in the computer generated cluster.

Tetrahedral sites in the cluster were filled with hydrogen sequentially according to the calculated binding energies E_b for each site and with an imposed H-H exclusion distance(blocking interaction) which was adjusted so that the final H/M value agreed with the experimentally measured H absorption. They concluded that $4 - Zr$ sites were completely filled and , $1Ni - 3Zr$ and $2Ni - 2Zr$ sites were partially filled at standard temperature and pressure. This conclusion is consistent with the results of Suzuki et al..

The first work on Ti-Cu glass alloys was by A.J. Maeland et al. In contrast to Ni-Zr metallic glasses, amorphous Ti-Cu had larger hydrogen absorption capacities and hydrogen diffusivity than the crystalline counterparts[10]. There is also some evidence of hydrogen-induced phase separation in this alloy.

As stated in the introduction, the electrochemical method is convenient for measuring the chemical potential and diffusion of hydrogen in metals. Much work exists for crystalline metals by this method. For amorphous metals, however, the application of the method is still rare.

Kirchheim et al.[8] carried out the first electrochemical measurement of hydrogen in amorphous metals. They investigated the chemical potential versus hydrogen content in amorphous $Pd_{77.5}Cu_6Si_{16.5}$ and $Ni_{49.9}Pd_{31.8}P_{18.3}$. By assuming a distribution in binding energy of hydrogen, their results indicated that the distribution is a single Gaussian distribution. By determining occupation probabilities using Fermi Dirac function (approximated as a step function), these workers derived the following expression relating H concentration C_H to G_0 and σ,

$$2C_H = 1 \pm erf[(G_0 - \mu_H)/\sigma] \tag{2.2}$$

with (+) for $G_0 < \mu_H$ and (-) for $G_0 > \mu_H$. By comparing this expression to their electrochemical free energy measurements of μ_H vs. C_H, Kirchheim et al. obtained a very good fit to Spit's data for $Ni_{64}Zr_{36}$ with the values $G_0 = 2.4KJ/mol - H$ and $\sigma = 17.5KJ/mol - H$, and for $Ni_{62}Ti_{29}Zr_9$ good agreement was found for $G_0 = 17.5KJ/mol-H$ and $\sigma = 15.5KJ/mol-H$. They interpreted this broad distribution as due to hydrogen in a distinct local chemical environment but with topological disorder resulting from the amorphous structure. In keeping with this interpretation, they related the width of the distribution σ to the width Δ and location r_o of the first peak in the RDF for the pure amorphous alloy(which reflects the distribution of distances between first nearest neighbors), the alloy's Young's modulus E_y, and the partial molar volume of hydrogen V_H through the expression

$$\sigma = E_y V_H \Delta / r_o \tag{2.3}$$

Their later results on amorphous $Ni_{35}Ti_{65}$[26] indicated a rapid increase in the slope of the open circuit potential versus hydrogen loading near H/M=0.25, which they interpreted as a shift from the filling of hydrogen states surrounded by 4 Ti atoms to the filling of higher energy sites associated with 3 Ti atoms and 1 Ni atom. They also studied amorphous Pd-Si system[29]. There is evidence that at higher hydrogen concentration($H/Pd > 0.2$), nearest-neighbor repulsive H-H interactions become important. No plateau was observed in the p-c isotherms. In 1984, they [31] investigated hydrogen in liquid-quenched and vapor-quenched amorphous $Pd_{80}Si_{20}$(the chemical potential, diffusion coefficient and partial molar volume). There were some differences between samples which were prepared by melt-spun and by sputtering, which were explained by assuming an energy distributions of greater width in the sputtered sample.

Harris et al.[32] reported electrochemical measurements of the EMF versus H/M in amorphous $Ni - Zr$ and $Pd - Ti$ over a wide range of composition. They charged the sample with hydrogen until H_2 gas was evolved at the surface. By open circuit measurement they can get the upper limit of measurable chemical potential μ_H in this method ($P_{H_2}^{max} = 1$ atm). Then a anodic current pulse was applied to extract a small, known quantity of hydrogen, followed by a open circuit reading to obtain μ_H at new H/M value. This procedure was repeated until the hydrogen concentration was so low that the time required for the sample to reach equilibrium(controlled by the diffusion of hydrogen) became impractically long. Thus, they measured only the hydrogen that cycled in or out of the sample within a window of chemical potential. Then they normalized the change of hydrogen concentration by the total reversible hydrogen. They found a universal feature that when scaled with the total reversible hydrogen, $\mu_H(H/M)$ has the same behavior. They then proposed a global model for H storage. and concluded that within their window of chemical potential, hydrogen is stored in tetrahedral site containing of 2Ni atoms and 2Zr atoms in Ni-Zr and in tetrahedra consisting of 1 Pd atom and 3 Ti atoms in PdTi. This conclusion for NiZr however is not consistent with either the results of Suzuki et al. or of Batalla et al..

2.3 Diffusivity

A very wide variety of experimental technique have been used to measure hydrogen diffusion in crystalline metal hydrides. Since about 1980, some of these methods have been applied to the study of diffusion in amorphous alloys and hydride phases[35]. Results were obtained from the kinetic rates for hydrogen absorption/desorption, electrochemical methods; from mechanical relaxation phenomena that are associated with short range reorientations of point defects or long range dilatational stresses ; from nuclear magnetic resonance (NMR); and from quasi elastic neutron scattering. Descriptions of all these procedures are beyond the scope of this introduction and just the results and discussions are reviewed.

In two respects, the diffusion behavior of hydrogen in amorphous metals is different from that in their crystalline counterparts:

(1) In crystalline hydrides, the mobility of hydrogen decreases with increasing hydrogen concentrations (larger than dilute limit), because with a single activation energy, the possibility that a hydrogen atom can jump to its nearest neighbor decreases with the increasing hydrogen concentration (because of blocking factor). In amorphous hydrides, however, the hydrogen diffusion coefficient often increases very rapidly with hydrogen content. In amorphous Pd-Si for example, the diffusion constant of hydrogen increases, even when the hydrogen concentration H/M changes from 10^{-5} to 10^{-3}[28], in contrast to the case of Pd where the diffusion coefficient is constant in the same hydrogen concentration region (dilute).

(2) In crystalline metals the measured diffusion coefficients D(T) often follows the Arrhenius relation:

$$D(T) = D_0 exp(E_D/kT) \tag{2.1}$$

Where D_0 the diffusion coefficient at 0K, and E_a the activation energy for the hydrogen diffusion process. However, in amorphous alloys, Arrhenius behavior is not generally observed.

Non-Arrhenius temperature dependences of the NMR relaxation times were first reported for amorphous $TiCuH_{1.3}$, $Zr_{65}Pd_{35}H_x$ and $Zr_2PdH_{2.9}$[35](see Fig.2.1). Two or more E_a values were needed to fit the data over the entire temperature regions. By comparison with the results for corresponding crystalline hydrides, it was suggest that hydrogen diffusion in the above amorphous hydrides probably consisted of a few discrete types of jump process each with a characteristic activation energy[36].

A fundamentally different approach to represent the non-Arrhenius behavior in the internal friction curves and NMR relaxation times is by a distribution of diffusion activation energies around a mean (or peak) value E_p as proposed by Kirchheim et al.[8]. The basic premise of this model is that the local environments for the interstitial hydrogen atoms vary in a quasi-continuous manner because of disorder in the glassy metal These variations will influence hydrogen diffusion through differences in the interstitial binding energies and the over the barrier energy for classical hopping processes This model reproduced the concentration and temperature dependences of both hydrogen solubility and diffusion properties as measured in several glassy metals when $H/M < 0.1$[8]. Numerical simulations by several research groups have shown the plau-

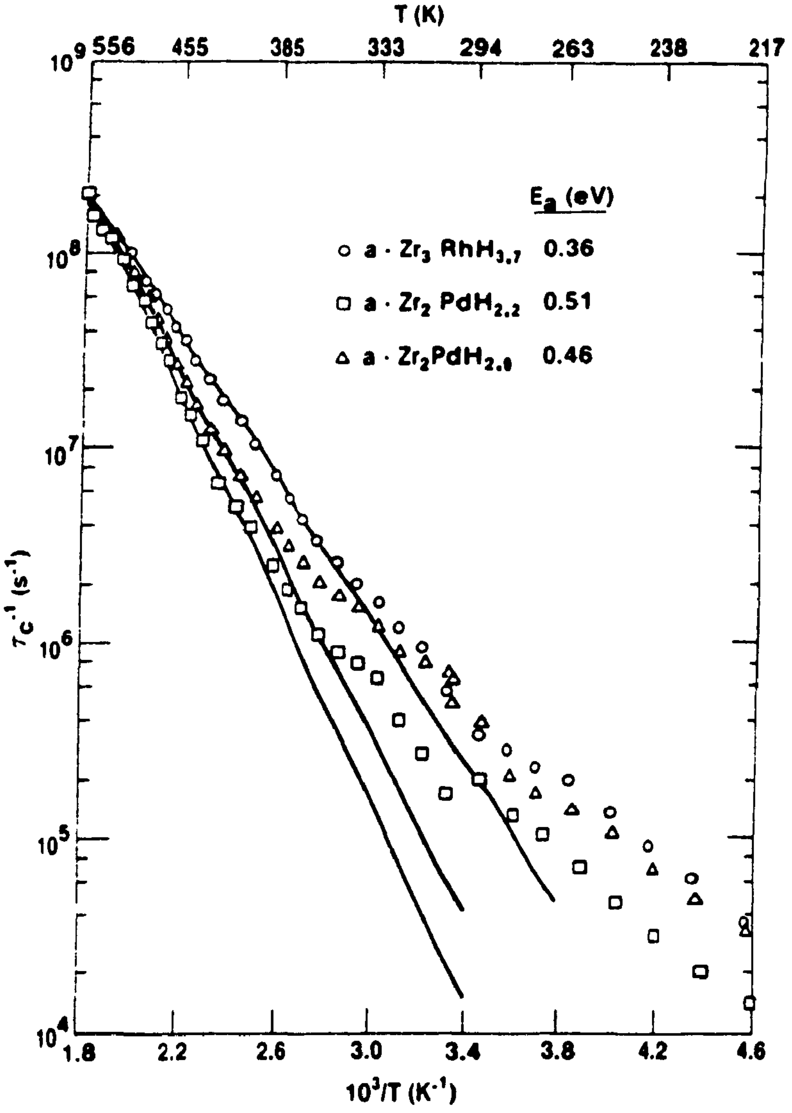

Figure 2.4: Temperature dependent behavior of the τ_c^{-1} parameters that were obtained by BPP-model analysis of the proton T_{l0} data for the three amorphous hydrides. The systematic deviations from Arrhenius straight lines are quite apparent(from reference[35])

sibility of energy dependent distributions of hydrogen site occupancies at the higher hydrogen concentrations as shown before[38, 17, 37, 30, 32]. The implications of such distributions to diffusion behavior would be non-Arrhenius temperature dependences if the energy distribution was sufficiently broad. In fact, the resonant frequency and temperature dependences of the proton relaxation times obtained from several amorphous hydrides have been analyzed with empirical distribution functions for E_a[41] Consequently, although an E_a distribution does give much better fits than any single-value Arrhenius relation, all the proton relaxation times still cannot be simultaneously fitted to within the precision of the experimental data[41]. On the other hand, the simple assumption of discrete temperature dependent E_a values also appears inadequate in light of the more recent results obtained with the distribution function models(mainly the concentration dependence). Lee and Stevenson[42] reported that an activation energy decrease also accompanied the increases in diffusion rates for amorphous $Pd_{1-y}Si_yH_x$ and $Ti_{52}Cu_{48}H_x$. In the few studies that compared hydrogen diffusion properties for crystalline and amorphous alloys greater mobility and smaller average E_a values were found for the glassy samples as long as $H/M > 0.01$. However, additional comparisons should be made before this behavior is regarded as a general trend. Clearly more work is needed to resolve this dilemma.

2.4 Summary

Various experiments have shown that there are significant difference between hydrogen in an amorphous and a crystalline metal. In an amorphous material a broad continuous distribution of interstitial site energies is expected whereas in a crystalline material a discrete spectrum of interstices is present which in most cases are well separated in their site energies. Hydrogen prefers to occupy early transition metal(ETM) sites or ETM rich sites.

In contrast to the extensive determinations of the p-c-t relationships for crystalline hydrides, the hydrogen absorption-desorption isotherms for only a limited number of metallic glasses have been reported. These alloys include: $Ni-Zr$, $Pd-Si$, $Ti-Fe$, $Ti-Cu$, $Ti-Ni$, and $Hf-Ni$. In several instances, the p-c-t isotherms from crystalline and amorphous alloys with equivalent compositions were directly compared. The main feature of the p-c isotherms are as follows. First, the maximum hydrogen stoichiometry is often smaller for the glassy alloy than for the crystalline alloy which suggest that the disorder usually place additional restrictions on favorable site occupancies. For example, neutron scattering experiments on amorphous $Ni_{50}Zr_{50}H_x$ indicated that only 4-atom coordination sites(i.e., Zr_4 and Zr_3Ni) are occupied while the crystalline hydrides $NiZrH_x$ phases will contain hydrogen atoms in Zr_4, Zr_3Ni, and Zr_3Ni_2 sites to give a larger total stoichiometry. Second, the slope $dP/d(H/M)$ is very large over the range of accessible pressures. In addition, at fixed pressure the H concentration increases with increasing ETM content. Finally, at fixed pressure and ETM content, the H concentration decreases rapidly with increasing temperature. Up to now, no plateau corresponding to a phase transition has been found in the p-c isotherm of any amorphous alloy even though they are clearly present for the corresponding crystalline system. Theoretical work by Griessen [37] and by Richards [30] has shown that for a site energy distribution of width $\triangle \geq 4kT_c(0)$, the critical temperature T_c is greatly reduced from its value of $T_c(0)$ at $\triangle = 0$ so that no phase transition could appear at general conditions.

Diffusion data of hydrogen in amorphous alloys is rare. However, we can still get some general idea. Diffusion experiments show that the Arrhenius relation is not generally valid[36]. The concentration dependence of diffusion coefficient of hydrogen in amorphous alloys is always strong and positive which is in contrast to the behavior of hydrogen in crystalline alloys. In some cases hydrogen diffusion in amorphous alloys is faster than it in crystalline alloys, in most cases it is slower

A Gaussian distribution of site energies(or several distributions), can be used to model the concentration dependence of the chemical potential of hydrogen and its diffusivity in amorphous metals. More careful work is needed for the complete understanding of hydrogen action in amorphous alloys, especially for hydrogen diffusion, and solubility which we will discussed in this thesis.

Chapter 3

Experimental methods

3.1 Electrochemical principles

When two electrodes are immersed in an electrolyte, a potential difference will arise between them. This potential difference depends on the reaction itself and the concentration of reactants and products in the solution.

3.1.1 Standard Hydrogen Electrode (SHE)

Since we can only measure a potential difference, the potential of a given electrode will have an arbitrary zero. One electrode reaction , which occurs when hydrogen gas at 1 atm is bubbled over the surface of a platinum sheet immersed in a 1M HCl solution (called standard hydrogen electrode (SHE)), is commonly chosen as zero. The reaction for the SHE is

$$H^+ + e^- \rightleftharpoons \frac{1}{2}H_2 \tag{3.1}$$

The potential of other electrode reactions are then measured relative to this SHE (at the same temperature). Since the SHE needs bubbling of hydrogen on the electrode surface, it is not easy to use.

3.1.2 Calomel Electrode

To determine the concentration dependence of the potential for a reaction, we begin with the reaction of a calomel electrode which we used as a reference.

$$Hg_2Cl_2 + 2e^- \rightleftharpoons 2Cl^- + 2Hg \tag{3.2}$$

The molar Gibbs free energy or chemical potential of ions μ, in a dilute solution is related to its molar concentration [M] by[44]

$$\mu - \mu_0 = RT\ln[M] \tag{3.3}$$

Where μ_0 is arbitrary, usually chosen as zero when $[M] = 1$. More precisely, [M] should be replaced by the activity of the ion in the solution. However since we are considering only dilute solutions where the interaction between the ions can be neglected, using [M] is a good approximation. Because 1 mole Hg_2Cl_2 has to produce 2 moles of Cl^- and 2 moles of Hg, a virtual change at the constant temperature and molar concentration(or pressure in gas case) will cause a virtual change in Gibbs free energy δG as

$$\delta G = \mu_{Hg_2Cl_2}\delta n_{Hg_2Cl_2} + \mu_{Cl^-}\delta n_{Cl^-} + \mu_{Hg}\delta n_{Hg} = \delta n_{Hg_2Cl_2}[\mu_{Hg_2Cl_2} - 2\mu_{Cl^-} - 2\mu_{Hg}] \tag{3.4}$$

Using eq.(3.3), we have

$$\delta G = \delta n_{Hg_2Cl_2}\Delta\mu_0 + \delta n_{Hg_2Cl_2}[RT\ln\frac{[Cl^-]^2[Hg]^2}{[Hg_2Cl_2]}] \tag{3.5}$$

Where $\delta n_{Hg_2Cl_2}\Delta\mu_0$ is a constant term of energy change, which depends on the materials involved in the reaction and the reaction itself. Because Hg_2Cl_2 and Hg are not soluble, their concentration in the solution is very small, so these two terms will contribute a constant value 2RT to the free energy change which can be included in δG_0. So the concentration dependence for the free energy change of the calomel electrode will be

$$\delta G = \delta n_{Hg_2Cl_2}[\Delta\mu_0 + 2RT\ln[Cl^-]] \tag{3.6}$$

Except for temperature, the free energy change will depend only on the molar concentration of Cl^-, which can be controlled by controlling the concentration of potassium chloride in the solution.

Since $\delta n_{Hg_2Cl_2}$ change of Hg_2Cl_2 in the reaction (3.2) neeas $2\delta n_{Hg_2Cl_2}$ of electron exchange, the energy change in such virtual change is (according to Faraday's law)

$$\delta G = -2FE\delta n_{Hg_2Cl_2} \tag{3.7}$$

Where F is Faraday's constant and E is the electric potential of this calomel electrode. Eq.(3.4) should be identical to eq.(3.7). Therefore, the electric potential of the calomel electrode will be

$$E = E_0 - \frac{RT}{F}\ln[Cl^-] \tag{3.8}$$

This equation is called the Nernst equation. At room temperature, and in saturated potassium chloride solution, the electrode potential of reaction (3.2) is +267 mv relative to SHE.

3.1.3 The Reaction of Hydrogen with Metal

The hydrogen atom usually can occupy an interstitial site of the host metal because it is very small relative to metal atoms. Therefore, the metal-hydrogen system can be thought of as a solid solution. The reaction for hydrogen loading of a metal is, then:

$$M + H_2 \rightleftharpoons M + 2H \tag{3.9}$$

The chemical potential of hydrogen in the gas phase, is related to its pressure p_{H_2} by

$$\mu = \mu_0 + RT \ln p_{H_2} \tag{3.10}$$

(assuming hydrogen is an ideal gas) The virtual free energy change of this reaction may be shown in a similar way to eq.(3.6) to be;

$$\delta G = \delta n_{H_2} [\Delta\mu_0 + RT \ln \frac{[H]^2}{p_{H_2}}] \tag{3.11}$$

The usage of [H] in eq.(3.11) has included the following assumption:

1. Every hydrogen atom inside the metal has the same binding energy (or in other words, they are identical) so that eq.(3.3) can be used.

2. The interactions between hydrogen atoms have been ignored, otherwise we have to use activity instead of [H]. This approximation valids at small hydrogen concentrations. When hydrogen concentration is high, eq.(3.3) will not valid.

Since the molar density of the metal is constant at a given temperature, [H] can be replaced by the atomic ratio of hydrogen and metal, c_H, with a constant added to $\Delta\mu_0$ because of this change unit. The term in *ln* is called the *reaction constant* for the reaction. It is a constant at a given temperature.(We can easily understand this by examining the condition for equilibrium. Under constant temperature and pressure, the Gibbs free energy must be a minimum. So from eq.(3.11) we find $\Delta\mu_0 = -RT \ln \frac{c_H^2}{p_{H_2}}$. Since $\Delta\mu_0$ depends only on T , this implies that the reaction constant depends only on temperature.) Therefore the concentration of hydrogen in the metal should be proportional to the square root of the hydrogen pressure outside the metal($c_H = (Kp_{H_2})^{\frac{1}{2}}$, K-the reaction constant). This is called Sievert's law[45], and is the first direct evidence that hydrogen exists in the metal in its atomic form.

From above calculations, it can be noted that Sievert's law can only be applied for crystalline materials which have a single binding energy for hydrogen, and when the concentration of hydrogen in the metal is small, so that the interaction between hydrogen atoms can be ignored and the activity of hydrogen in the metal can be replaced by its concentration in eq.(3.3). In amorphous metals, there is usually no single binding energy for hydrogen as we mentioned in Chapter 2, and Sievert's law is not expected to hold. If the hydrogen concentration is high, the approximation of using molar concentrations in eg.(3.3) is not valid, and we have to use activity instead of concentration. There are theories (Debye-Huckel theory)[40] to calculate the activity coefficient f, which is the ratio of activity to concentration, by including the interaction between hydrogen atoms (hydrogen atom in the metal may be partially ionized, see the introduction in ref.[5]). It can also be measured by experiment. When calculating the interactions between hydrogen atoms, the effects of metal must be considered and the calculation may become very complicated. The activity of hydrogen atoms is usually not linearly proportional to its concentration at high hydrogen concentrations. Sieverts' law will no longer be obeyed. Bat·lla et al. [17] gave a calculation of hydrogen binding energy for amorphous $Ni-Zr$.

We now turn to the electrochemical loading of a metal by hydrogen, assuming again that the metal-hydrogen system can be treated as solid solution. The overall reaction for H^+ rich electrolyte can be written as

$$M + H^+ + e^- \rightleftharpoons M + H \tag{3.12}$$

Because the electrolyte is H^+ rich, the concentration of H^+ is essentially constant. Following similar calculations as we did before, we can easily show

$$E = E_0 - \frac{RT}{F} \ln c_H \tag{3.13}$$

For OH^- rich electrolyte, the overall reaction is different and is written as

$$H_2O + M + e^- \rightleftharpoons H + OH^- + M \tag{3.14}$$

However, since the chemical potential of H_2O does not change, the concentration of OH^- is constant, and the electric potential has the same form as eq.(3.13).

The above is only the equilibrium case; the real system is not always in equilibrium. It is convenient to define a second quantity Q such that

$$Q = c_H \mid_a \tag{3.15}$$

Here, the subscript a indicates that the concentrations are instantaneous concentrations and not equilibrium concentrations. The quantity Q, therefore , is not a constant, but changes continuously until equilibrium is reached; at that point, Q becomes equal to c_H and the subscripts are deleted. From thermodynamics, it can be shown that the change in chemical potential $\Delta\mu$ due to this nonequilibrium process is given by

$$\Delta\mu = RT \ln Q - RT \ln c_H \tag{3.16}$$

Then we have

$$\Delta E = -\frac{RT}{F} \ln Q + \frac{RT}{F} \ln c_H \tag{3.17}$$

The last term is called the *standard potential.*

Since the reaction happens at the interface between electrolyte and metal electrode, the rate at which the system reaches equilibrium will depend on the diffusion rate of hydrogen in the metal bulk. The simplest model that describes this diffusion is that of linear diffusion in a plane electrode. It is assumed that the electrode is perfectly flat and of infinite dimensions, so that concentration variations can only occur perpendicular to the electrode surface. Diffusion may then be characterized by Fick's laws in a one dimensional form as:

$$\frac{\partial^2 C}{\partial x^2} - \frac{1}{D}\frac{\partial C}{\partial t} = 0 \tag{3.18}$$

Where C is concentration of hydrogen , D the diffusion coefficient.

With different initial and boundary conditions, various solutions of the above equation are known. The double cell technique is a convenient method to set and control the boundary conditions.

3.1.4 Double Cell Technique

This technique uses two identical cells each equipped with a reference electrode, a counter electrode, and a common working electrode (details of the design will be described in Section 3.3; the experiment set-up). Since the potential of the reference electrode is a constant, we can control the potential of the working electrode through external circuit by referring to the reference electrode. Two methods are often used: potentiostatic and galvanostatic method.

Potentiostatic method

Initially, both sides of the working electrode (the sample) are controlled by a potential (between reference and working electrode) which makes the surfaces free of hydrogen (the current is very small). After the system reaches equilibrium, the potential of the entry side of the working electrode is switched to a new value which charges the working electrode with hydrogen. The current in the charge cell will increase abruptly, while in the discharge cell, after a short delay, the current will increase slowly. If we assume that any variation of surface coverage with hydrogen results in an instantaneous changes of hydrogen concentration just below the surface of the metal, and that there is no current between the reference electrode and the working electrode to cause an overvoltage, then the hydrogen concentration, although not in equilibrium, will be a constant if the potential at this side is constant The boundary condition of above process will be

- Initial conditions: $c(0,t) = c_0$, constant, $x = 0$, $t > 0$

3.1.4 Double Cell Technique

This technique uses two identical cells each equipped with a reference electrode, a counter electrode, and a common working electrode (details of the design will be described in Section 3.3; the experiment set-up) Since the potential of the reference electrode is a constant, we can control the potential of the working electrode through external circuit by referring to the reference electrode. Two methods are often used: potentiostatic and galvanostatic method.

Potentiostatic method

Initially, both sides of the working electrode (the sample) are controlled by a potential (between reference and working electrode) which makes the surfaces free of hydrogen (the current is very small). After the system reaches equilibrium, the potential of the entry side of the working electrode is switched to a new value which charges the working electrode with hydrogen. The current in the charge cell will increase abruptly, while in the discharge cell, after a short delay, the current will increase slowly. If we assume that any variation of surface coverage with hydrogen results in an instantaneous changes of hydrogen concentration just below the surface of the metal, and that there is no current between the reference electrode and the working electrode to cause an overvoltage, then the hydrogen concentration, although not in equilibrium, will be a constant if the potential at this side is constant. The boundary condition of above process will be

- Initial conditions: $c(0,t) = c_0$, constant, $x = 0$, $t > 0$

- Boundary conditions:

  Entry face: $c(x,0) = 0,\ 0 < x < l,$

  Exit face $c(l,t) = 0,\ x = l,\ t > 0$

Where l is the thickness of the electrode.

The solution can be written as[5]:

$$J_t = \frac{2D^{\frac{1}{2}}c_0}{(\pi t)^{\frac{1}{2}}} \sum_{m=1}^{\infty} (-1)^m e^{-(m-\frac{1}{2})^2 l^2/Dt} \tag{3.19}$$

and taking:

$$J_\infty = \frac{Dc_0}{l} \tag{3.20}$$

We have:

$$\frac{J_t}{J_\infty} = \frac{2l}{(\pi D t)^{\frac{1}{2}}} \sum_{m=0}^{\infty} (-1)^m e^{-(2m+1)^2 l^2/4Dt} \tag{3.21}$$

where $\frac{J_t}{J_\infty}$is the fractional attainment of steady state of the flux through the thin metal foil. If the diffusion rate does not depend on hydrogen concentrations, we can reasonably assume, for the above boundary conditions, that the steady state concentration profile is linear. We can then estimate the average hydrogen concentration from J_∞. Fitting to the time dependence of the transient at exit side, diffusion coefficient can be obtained. (In fact the discharge side need not be free of hydrogen. It may be held at a constant potential so that the concentration is a constant value c'. The difference in concentration between the two sides still satisfies the first boundary condition.)

Galvanostatic method

Initially, both sides of the working electrode is also controlled to be free of hydrogen. Then a constant current is applied to the charge side. After a while, the current at exit side will rise. The boundary condition now is:

- Initial conditions: $D(\frac{\partial c}{\partial x})_{x=0} = j$, constant, $t > 0$
- Boundary conditions:

  Entry face: $c(x,0) = 0,\ 0 < x < l$

  Exit face: $c(l,t) = 0,\ x = l,\ t > 0$

and the solution is[5]:

$$\frac{J_t}{J_\infty} = 1 - \frac{4}{\pi}\sum_{m=0}^{\infty}[(-1)^m/(2m+1)]exp[-\pi^2(2m+1)^2Dt/4l^2] \qquad (3.22)$$

Where J_∞ has the same meaning as eq.(3.20). The hydrogen concentration can be determined from J_∞, and diffusion constant can be obtained by fitting the transient at exit side.

These two methods have a common defect: the system is not in equilibrium during the measurement, and so cannot be used to determine the chemical potential of the reaction. Also there is a large gradient of hydrogen concentration through the sample, so one cannot measure the diffusion coefficient in materials where the diffusion constant changes rapidly with hydrogen concentration. However, it is possible to measure both the chemical potential and diffusion coefficient more exactly using an alternate method, the current pulse technique.

Current pulse technique

A single current pulse of height i_0 and duration t_0 is sent through the charge side of the cell (initially both cells are kept open circuit and stable). After switching off the current(open circuit at both sides) the following boundary conditions are fulfilled

- Boundary conditions:

$$\frac{\partial C}{\partial x} = 0 \tag{3.23}$$

  for $x = 0$ and $x = s$ (at $t \neg 0$).

- Initial conditions: $c(x,0) = c_0 + g(x)$

  Where $g(x)$ is the non-uniform part of hydrogen distribution in side the metal just after the current pulse.

With a homogeneous concentration distribution in the beginning,$c(x,0) = c_0$, and a sufficiently short pulse-duration, Züchner [49] has obtained the following solution of eq.(3.18):

$$c_s(\tau) = c_0 + (c_\infty - c_0)[1 + 2\sum(-1)^N exp(-N^2\tau)] \tag{3.24}$$

where c_s is the hydrogen concentration at the detection side, c_0 the initial concentration, c_∞ the final concentration after equalization, and $\Delta c = c_\infty - c_0$. τ contains the diffusion coefficient, D, and the thickness of the sample, l as follows:

$$\tau = \frac{\pi^2 Dt}{l^2} \tag{3.25}$$

The hydrogen concentrations c_0 and Δc are related to the charge of the current pulses ΔQ by:

$$c_0 = \frac{Q_0 V_M}{F v_M}, c_\infty - c_0 = \Delta c = \frac{\Delta Q V_M}{F v_M} \tag{3.26}$$

where V_M is the molar volume of the working electrode, v_M the volume of the electrode and Q_0 the amount of hydrogen that is already in the sample.

Then we have (see eq.(3.16))

$$\begin{aligned} E(\tau) &= E(\tau = 0) - \frac{RT}{F} ln(1 + \\ & \frac{\Delta Q}{Q_0}(1 + 2\Sigma(-1)^N exp(-N^2\tau))) \end{aligned} \tag{3.27}$$

Where $E(\tau = 0) = E_0$ is the *equilibrium* electrode potential after precharging the sample, namely:

$$E_0 = E_0' - \frac{RT}{F} ln Q_0 \tag{3.28}$$

E_0' is the chemical potential of sample when no hydrogen exist in sample. When $t \rightarrow \infty$, E reaches a new *equilibrium* potential. So by measuring the chemical potential of the sample at the exit side, we can determine both the diffusion coefficient (by fitting to the transient) and the equilibrium potential at various hydrogen concentrations.

In fact, what we have considered is too simplified. We have not considered the effects of the electrolyte, and have assumed that all hydrogen atoms created in the reaction enter the metal electrode instantaneously and then only diffuse into the metal (i.e. do not come out again). These assumptions must be analyzed more carefully.

Microscopically the build-up of the potential difference between the electrode and electrolyte needs a thin double-layer of charge at the electrode surface. The movement of electrolyte fluid will cause the ions in the electrolyte to move, and this will affect the double layer and hence the potential difference. During a reaction, reactant ions trying to reach the electrode surface may experience mechanical forces, caused by an external potential (which gives a potential gradient in the electrolyte) or by a concentration gradient. To get rid of the complexity, we must choose the experimental conditions properly. Suppose the solution is not stirred. We then do not need to consider the effect of mechanical force. Suppose further that reactant ions in the solution move much faster than other kinds of ion, and are also very rich in the solution. We then do not need to consider the movement of the ions caused by the potential gradient (because enough reactant ions always exist near the electrode surface, and do not need a large electric force to push them to the electrode ; hence no potential gradient is needed.) Under these two conditions, diffusion is the only form of ionic motion in the electrolyte. Because the hydrogen ion moves much faster than any other kinds of ion, we can easily satisfy these two conditions by using unstirred acid electrolyte.

Basically, the diffusion rate determines the electrochemical reaction rate , because the faster the diffusion rate of a species ,the larger its collision probability. This property is very important in the selection of electrolyte. In addition to the reaction (3.12), there is also the possibility of hydrogen recombining with oxygen dissolved in the electrolyte. By chosing a high viscosity electrolyte(and so a low diffusion rate), this recombination reaction can be minimized. As was suggested by Kirchheim[8], a mixture of glycerin-phosphoric acid was chosen in this study. This choice also reduces the possibility of hydrogen molecules which may be formed (by a side reaction; $H^+ \rightarrow H \rightarrow H_2$)

at the electrode surface diffusing back into the electrolyte (Stokes-Einstein relation). The choosing of high a viscosity electrolyte should not influence the neutralizing of H^+ into H, because the process is under an external electric force.

The assumption that hydrogen diffuses only into the metal is a bit harder to justify, though it has proved to be a good approximation. We may understand this as follows: As H^+ is adsorbed on the metal surface, it picks up an electron which it shares with the bulk metal . It will then be hard for hydrogen to escape from the metal surface, but easy to diffuse into metal because it is already in a sense part of the metal.

Surface contamination

When the solvent molecules are bipolar, they may be oriented on the electrode surface. This will caused an extra nonreaction potential. The magnitude of such a potential will depend on the surface conditions, e.g. the material of the electrode, and the roughness of the electrode surface. This surface potential will influence the reaction. We have to eliminate it. As mentioned in introduction, by cleaning the electrode surface, the effect can be minimized, though it is impossible to overcome it completely. Some further discussion will be given in Chapter 4.

3.2 Sample preparation

To get a homogeneous and large enough sample, a sputtering technique was used. By depositing materials on clean substrates, possible pin holes, that would make the diffusion measurement invalid, were eliminated. In addition, we can also use this technique to deposit a Pd layer on the sample surface.

The reason we need a thin layer of Pd is because of the oxidation of Ni-Zr leads to the formation of a ZrO_2 surface layer.

According to D. Khatamian and F.D. Manchester[48], hydrogen diffuses very slowly in ZrO_2 (at room temperature the diffusion constant is about $10^{-30}m^2/s$). This is so much slower than the $Ni - Zr$ bulk which we are going to study that even a thin layer of oxide will dominate the diffusion process, so making it impossible to deduce the diffusion rate in the bulk. It takes the same time for hydrogen to diffuse through a $1\AA$ thick layer of ZrO_2 as through a $1cm$ layer thick of $Ni - Zr$ This means that only for hydrogen diffusion in 1m thick sample of $Ni - Zr$, can the effect of 1 Åthick layer of ZrO_2 be ignored. Obviously, any study of hydrogen diffusion in bulk $Ni - Zr$ is impossible in practice (even prepared in high vacuum, there is about 10-50 Åof oxide layer on the surface) without proper treatment of the oxide layer. By coating the sample with a thin layer of Pd the sample is protected against the oxidation in sample preparation process and also facilitates the adsorption of hydrogen on the sample surface[41].

Using the sputtering facilities available, it was not possible to coat the sample with Pd without removing it from the vacuum. Fortunately, Pd is not easily oxidized, so we can sputter a film of Pd and then deposit $Ni-Zr$ by sputtering, and so get at least one side of the sample free of ZrO_2. This side is used as the exit side for hydrogen, since the large current and effectively high hydrogen pressure on the entry side easily breaks up the oxide layer on the uncoated side. With Pd coated on the ZrO_2 free surface of $Ni - Zr$, hydrogen should have no difficulty in going from the bulk $Ni - Zr$ to the Pd surface and so establish equilibrium with the outside. The Pd layer must be thick enough to inhibit oxidation, but not so thick as to dominate the chemical potential and concentration of hydrogen in the sample. 50-100 nm is a good value for 25 μm thick sample of Ni-Zr, because even if the hydrogen concentration (H/M) in such layer of Pd reaches 1 (this will correspond to very high hydrogen pressure in the p-c isotherms), the total hydrogen in the Pd, if distributed in Ni-Zr sample, will only contribute 2.5×10^{-3} in H/M (much smaller than the amount by one single charging step). The time it takes for hydrogen to diffuse through this thin layer of Pd can also be neglected, relative to the time for hydrogen to go through bulk Ni-Zr (It takes about a few mili-seconds for H to diffuse through this layer of Pd, but thousands seconds through Ni-Zr).

The sputtering system (fig.3.1) is a RF triode system with anode, filament, and ground. The target with diameter of 2 inches and thickness of 5 mm (shown in fig.3.2) was made of Ni(99.5%) plate and Zr(99.2%) rod. The composition of the sample was controlled by the relative area of Ni and Zr on the target, using the calibration data of the system[47]. By arranging for a symmetric distribution of Zr and Ni, the composition of the sample is uniform. The target was mounted on a copper housing with indium so as to ensure good electrical and thermal contact. The crystalline silicon substrate, of dimension $5 \times 3cm^2$, was cleaned carefully in acetone and then in propanol at temperature of about $40°C$ before being put in the system. It was set 5 cm above the target and attached to a water cooled support. The system was pumped to a vacuum

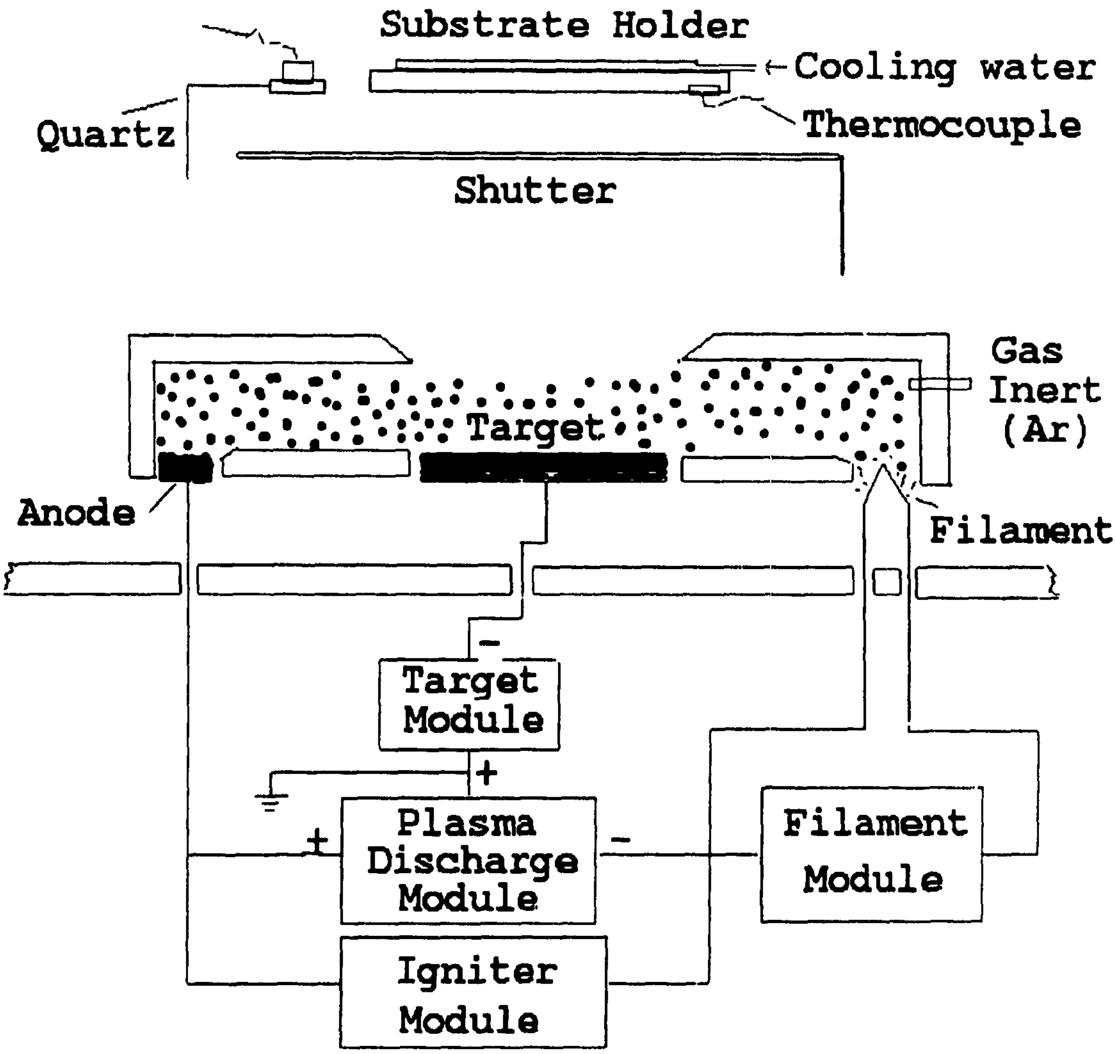

Figure 3.1: RF Sputtering System

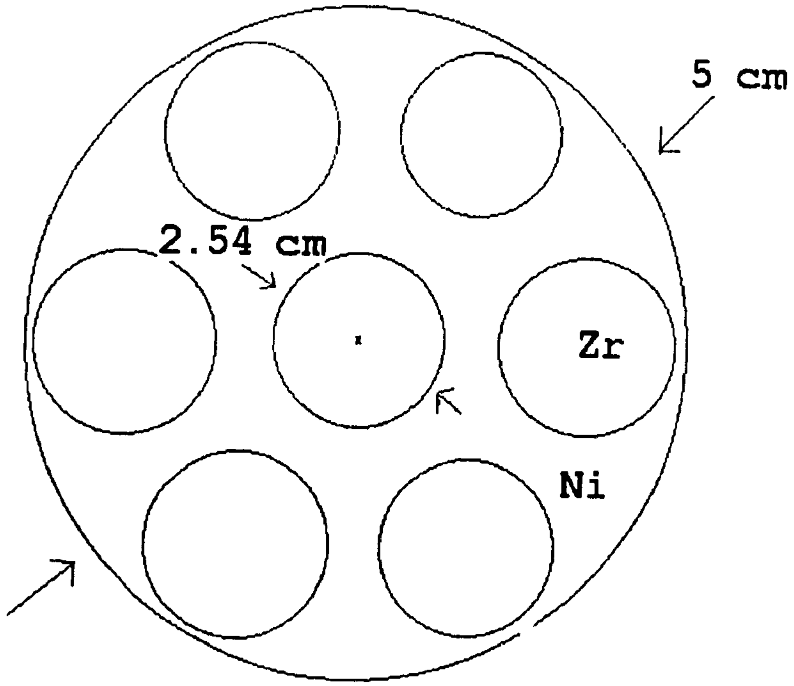

Figure 3.2: Target

of $10^{-10}Pa$, with an oxygen partial pressure of order $10^{-12}Pa$ The thickness of the sample was measured with quartz during the sputtering process. At a plasma power of 300 W, the depositing rate is about $100nm/s$. A thin layer of Pd(about 600A) was deposited first(target of Pd is 1 inch in diameter), then the vacuum was broken and the target changed so that $Ni - Zr$ could be deposited on this layer of Pd. Because of the thickness of our sample(about 25 μm) and the difference of expansion coefficient between Si and Ni-Zr, and also the internal strain in the amorphous alloys, the film can be gently removed from the substrate after the deposition.

The amorphous structure of the sample was confirmed by X-ray powder diffraction (shown in fig.3.3). At the surface with Pd, we see several sharp peaks that correspond to the texture of Pd(111). At the other side, it is the usual amorphous structure.

3.3 Measurement setup

Details of the electrochemical setup can be seen in Fig.3.4.

(1) The cell is made up of two pieces of transparent plexiglass tubes closed at one end, which can be mounted on a triangular channel so that they are coaxial.

(2) is a pair of calomel standard electrodes made in the laboratory. Details are shown in Fig.3.5. After grinding calomel, mercury, and a little saturated potassium chloride solution together, the resultant homogeneous slurry was placed in a layer of about 1-2 cm thick on the surface of pure mercury contained in a clean pytex tube with a short length of Pt wire through the bottom to permit electrical contact. The

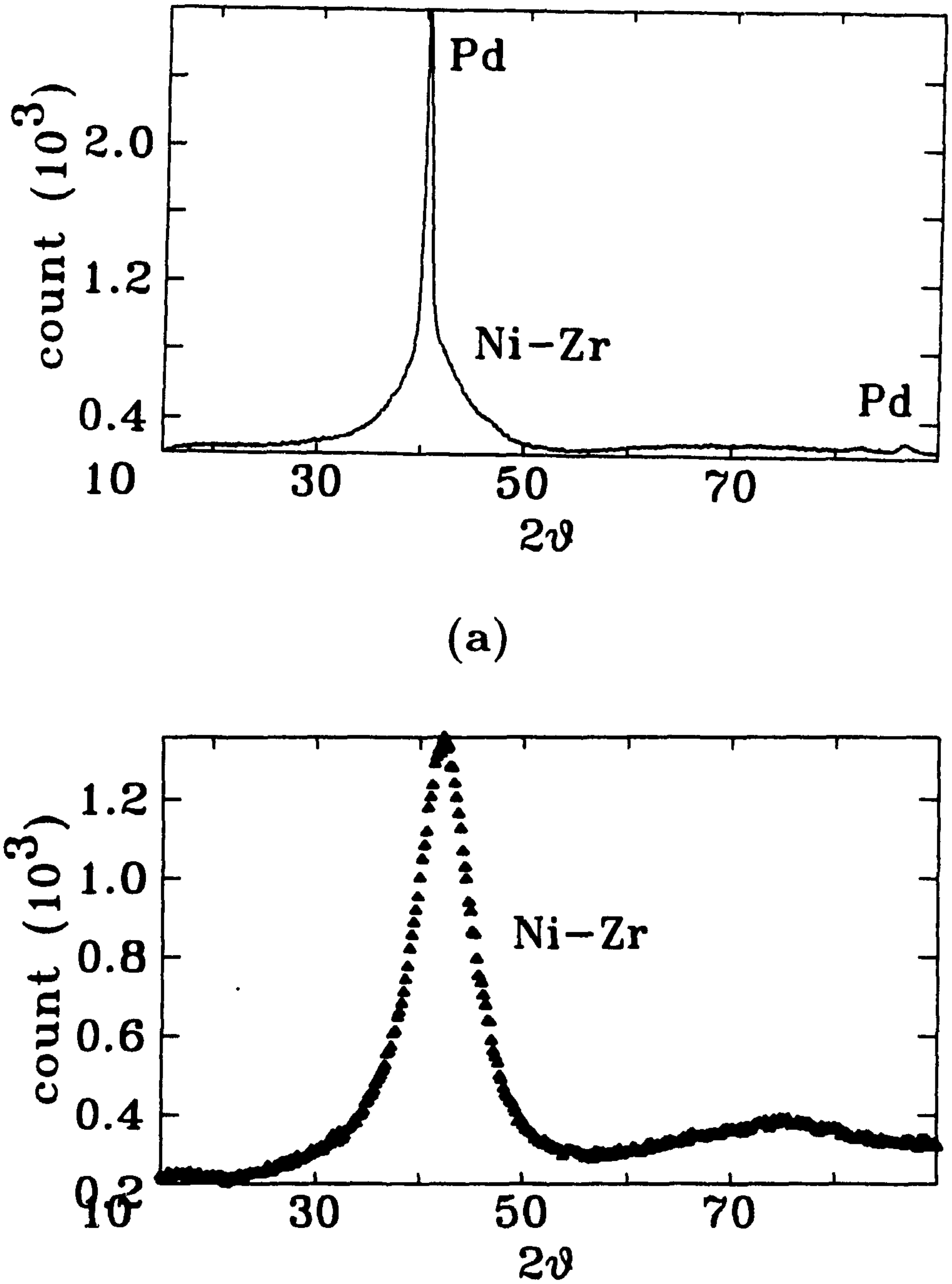

(a)

(b)

Figure 3.3: X-ray diffraction of the sample; (a) The face that have Pd (b) The face that have no Pd

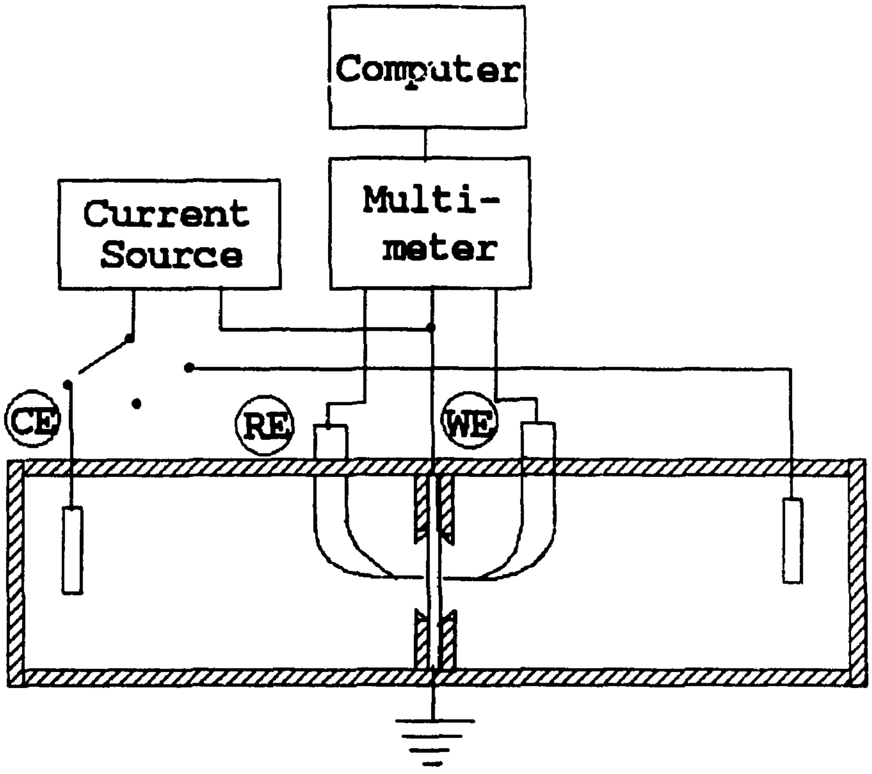

Figure 3.4: Experimental set-up

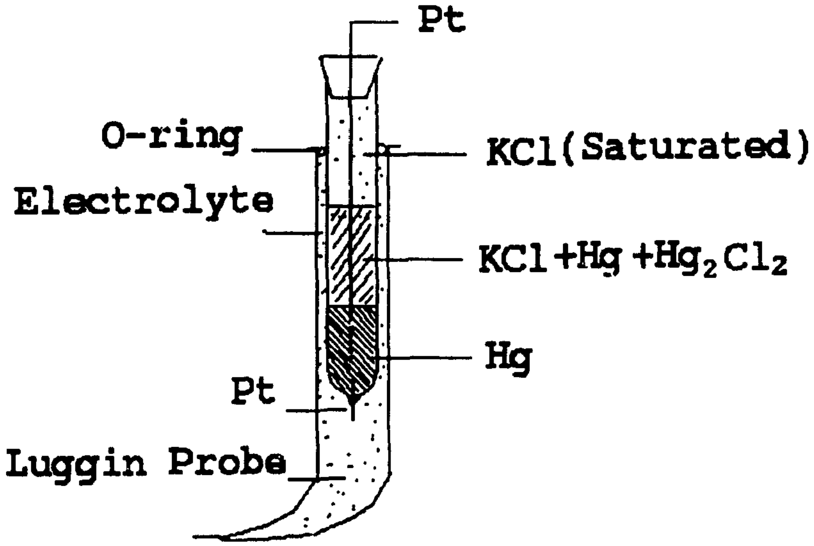

Figure 3.5: Calomel electrode

saturated potassium chloride solution was then added carefully into the tube. A *Pt* wire with thickness of about 0.127mm through a soft wood cap was dipped through the sandwich of KCl solution, Hg, and mixture of Hg, KCl, and Hg_2Cl_2.

Testing of the calomel electrode was done by measuring the potential between the calomel and standard hydrogen electrode in a 1M HCl contained test glass. The result of about $+270 \pm 5$ mV is, within error, the accepted value of 268 mV. No voltage difference was seen between the two calomel electrodes. implying that the two calomel electrodes are identical.

The salt bridge between calomel and cell is a Luggin capillary made up of thin-wall glass tube which changes abruptly from wide to capillary(to minimize the capacity between working and calomel electrodes) at its end and was made as close to the working electrode (sample) as possible.

(3) a *Pt* counter electrode plate, was used for doping the sample with hydrogen and was set about 8 cm away from the WE. This has the advantage of keeping any oxygen which may be formed during the reaction process at the Pt away from the WE. The choice of *Pt* plate rather then wire ensures a fast reaction.

(4) are two specially-designed washers. Upon absorption of hydrogen, the $Ni - Zr$ sample tends to expand(about a few percent in width and length). At the same time, the sample becomes somewhat brittle, and will therefore tend to crack when the content of hydrogen reaches a certain value, generally, about 20% in H/M(because the fracture strain of Ni-Zr decreases abruptly at 20%, see fig.3 6). To eliminate this, the washer was designed as shown (see fig.3.7). The curvature of it was calculated according to

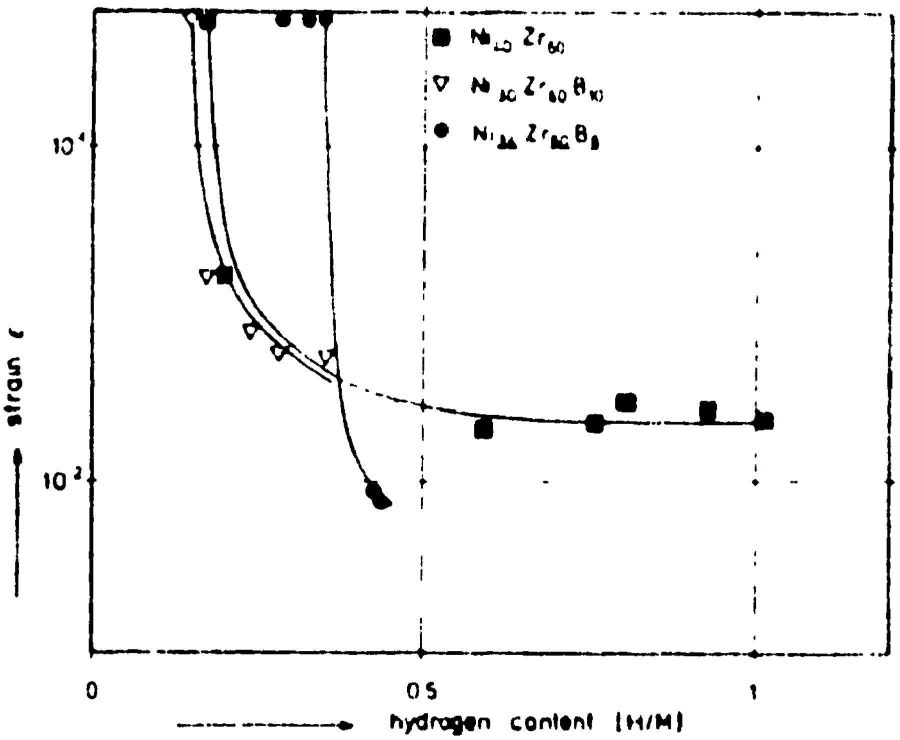

Figure 3.6: The fracture strain at various hydrogen concentrations for Ni-Zr-B metallic glasses from reference[46]

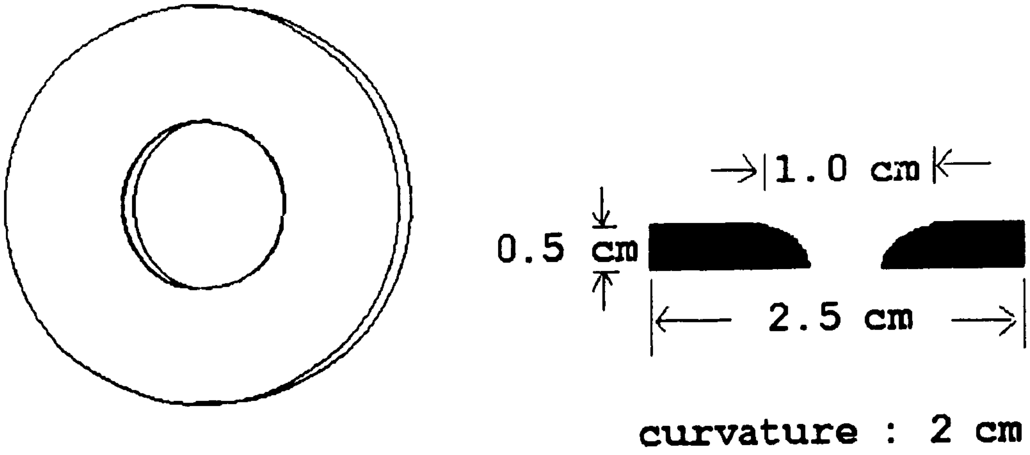

Figure 3.7: The design of washer

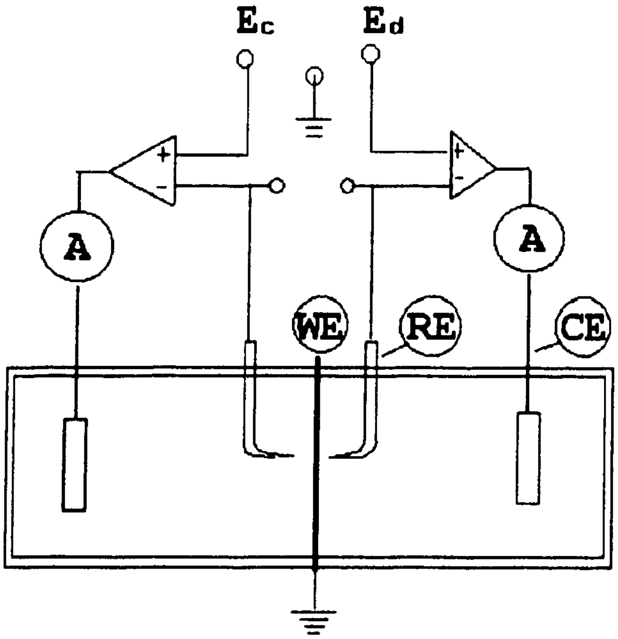

Figure 3.8: The circuit for potentiostatic method

$$\epsilon = \frac{d}{R} \tag{3.29}$$

where ϵ is the strain, d is the thickness of sample, R is the radius of the curve(about 1cm).

The electrolyte used in the current pulse technique was prepared by mixing two volume parts of glycerin with one volume part of phosphoric acid (85% wt.). This electrolyte is hygroscopic and has, therefore, to be renewed after several measurements.

The current source is standard Keithly 215 current source. The voltmeter we used is Keithly 199 multimeter with input resistance not less than $10^{10}\Omega$. Data was collected with IBM XT computer at designed interval through IEEE 488 interface. A stop watch was used to record the time or the amount of charge that was doped in the sample with certain current. Before using the current pulse technique, both the potentiostatic and galvanostatic methods were used to measure the diffusion coefficient of H in Pd and $Ni - Zr$ with electrolyte of 1M acetic acid. Electronic circuit is shown in Fig.3.8. The results of these methods will be discussed in next Chapter.

Chapter 4

Results and discussions

4.1 Testing of the apparatus

Pd foil of purity 99.9% with dimension $25 \times 25 \times 0.25mm^3$ (0.25 mm is the thickness) (supplied by Johnson Matthey) was used to test the apparatus. The foil was thick enough to minimize the risk of pin holes , but not so thick as to create large errors in the diffusion experiments, as discussed below.

Before mounting the foil in the cell, the Pd was cleaned to remove any surface contamination. First, it was baked at a temperature of about 600C for half a hour to drive off any residual hydrogen. It was then abraded in distilled water with emery paper to remove residue on its surface. Then the foil was immersed in acetone for about half a hour to dissolve any residue. Finally, the sample was washed in distilled water.

The Pd was then mounted between two washers with a hole 1 cm in diameter. After about two hours the voltage (or current) at both sides of the cell became stable (the variation of emf was less than 0.1 mv in fifteen minutes), the first charging process was started, data being collected by computer at typical time intervals of 10 seconds.

4.1.1 The Current-pulse technique

Current-pulses of 10mA to 15mA with a duration of a few seconds (less than 10 seconds) are applied at the entry side of the cell. The amount of charge is determined by measuring the time duration of the current. At the end of the pulse, both sides of the cell are returned to open circuit. Typically, after about one and half minutes, the potential of the exit side begins to change signalling the arrival of hydrogen. When the emf at the exit side saturates, another pulse is applied, and the cycle repeated. The transient is shown in fig.4.1. If saturation implies a uniform concentration of hydrogen, then there should be no potential difference between entry side and exit side. However, a small difference is seen. Fig.4.2 shows the difference in e.m.f. or potential between the entry and exit sides at various hydrogen concentrations. It can be seen that the difference decreases as the hydrogen concentration increases and tends to saturation at higher hydrogen concentrations (the saturated value is about 15 mV). This suggests that there are at least two mechanisms for the potential difference.

First, there may be a small hydrogen density gradient at the entry side, which may cause a small extra non-equilibrium potential when the potential at the exit side becomes saturated. Such small gradient arises from the competition between the normal forward diffusion and side-ways diffusion. The former process causes the ΔE at exit

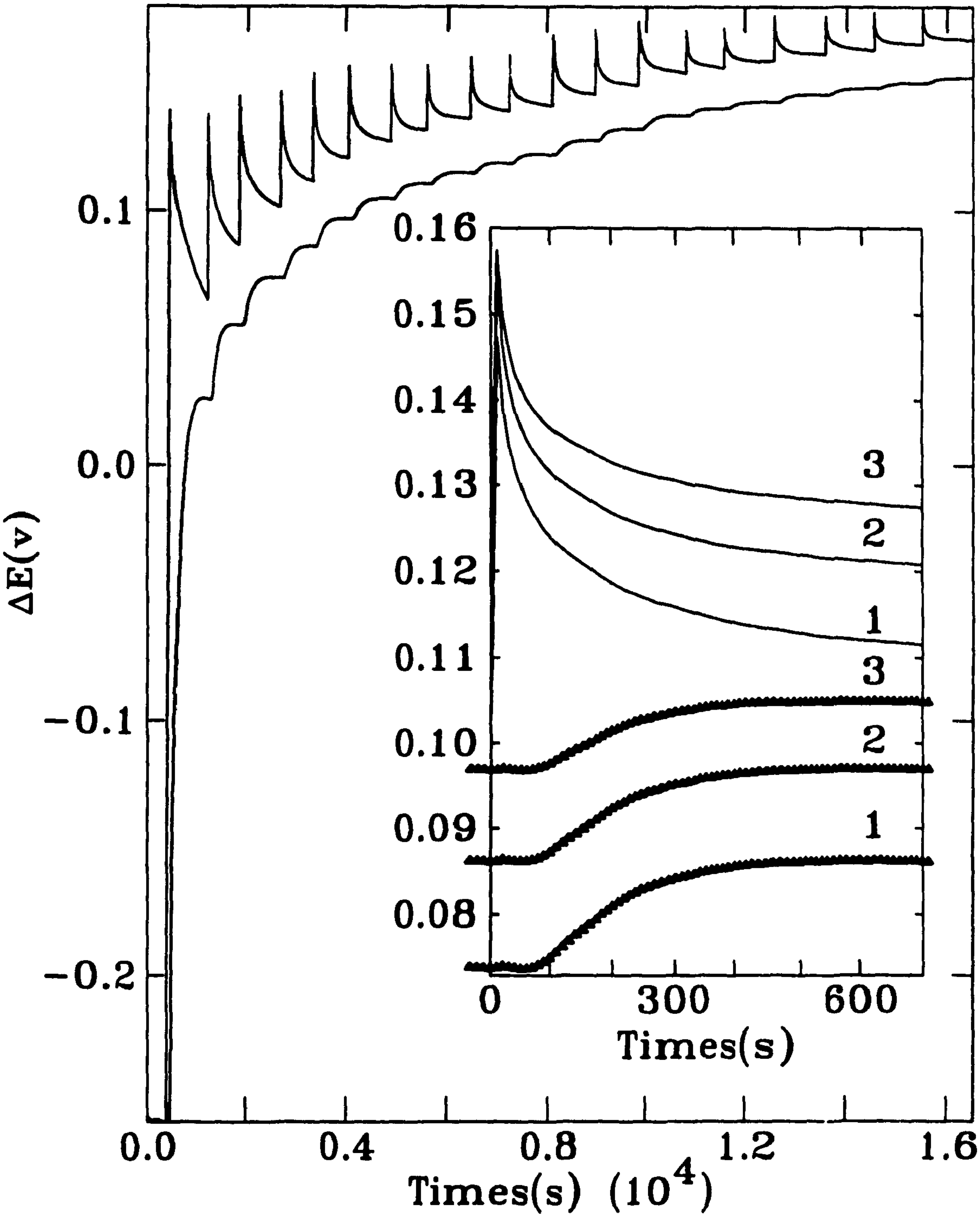

Figure 4.1: Typical transient of Pd in pulse current method

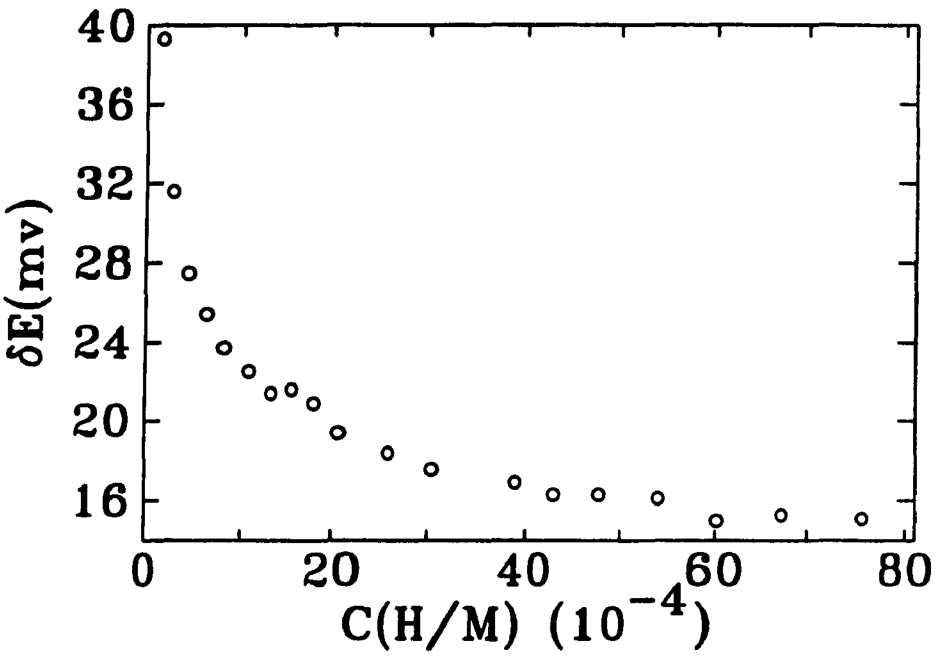

Figure 4.2: The e.m.f. differences between entry and exit side at various hydrogen concentrations for Pd

side to increase as we saw in eq.(3.28); the latter will cause the ΔE at both sides to decrease because of the lowering of hydrogen concentration. When these two effects balance, the ΔE at exit side saturates, while, there is still a small concentration gradient at the entry side. (After saturation, the forward diffusion of hydrogen becomes slower while the diffusion sideways is still large, so that the emf at the exit side will then decay. This phenomenon can be seen in fig.4.1 when the transient is enlarged. Thus, one cannot wait too long at the exit side to let the gradient of entry side cease.) Since the e.m.f. is related to the logarithm of the hydrogen concentration, the potential change, caused by one current pulse, will decrease when the total hydrogen inside the Pd increases. Therefore, the small gradient of hydrogen concentration at the entry side, which is dominated by the last charging process (because the previous gradient should have decayed during the last cycle), will contribute a even smaller value of e m.f. difference. Assuming that when the e.m f. at exit side saturated, the distribution of H is uniform, then hydrogen should have diffused, perpendicular to the normal diffusion direction, about a similar distance as the thickness of the sample. In other words, because of the side-way diffusion, the hydrogen will be distributed over an area larger than the charging area. This increase in hydrogen distribution area can effectively be described as an increase in the radius of the charging area. Thus, with a certain charging area, the thinner the sample, the smaller the broadening of hydrogen distribution. (That is why the sample can not be too thick). With a charging area of 1 cm in diameter and 0.025 cm in thickness, the loss in charging area due to diffusion side-ways will be about a few percent of the total H absorbed.

Second, the surface condition of two sides may be different. As was mentioned in Chapter 3, as well as the potential due to the reaction, there is surface potential which depends on the material of the electrode and the surface conditions (e g. the roughness). Thus, differences in surface condition may cause a potential difference. In fact, it was observed that when the Pd was removed from the cell, contamination of the entry surface was seen. This unknown contaminant proved difficult to wash off. From fig.4.2, it seems that such surface contamination causes a constant potential of 15mv. It should have no effect on the diffusion constant over the short time scale of the measurement, because we only need the emf changes to get the transient and hence the diffusion coefficient. In fact, as has been pointed out by Zuchner[49], surface impedances have no influence on the diffusion experiment by current pulse method, as long as it does not entirely prevent penetration of hydrogen into the metal.

The e.m.f. of Pd measured at exit side is shown in fig.4.3 for various hydrogen concentrations at T=298K (For convenience, we set zero as the potential of SHE. Higher pressure corresponds to higher value of e.m.f.. This applies to all of our results.). As can be seen, the slope of the straight line in fig.4.3a is RT/F as given in Chapter 3. (here, hydrogen is in α phase. The transition from α to β phase (a plateau at emf-c diagram) was seen by charging the Pd with small current (0.1 mA) at entry side, and measuring the emf at exit side for very long time (24 hrs) (see fig.4.3b).) This gives confidence in the measurements (and also agrees with the results in ref.[49]). Deviations of the data points from the straight line behavior are expected at low concentrations because of the presence of other reactions. (Obviously, in practice, when hydrogen concentration in the metal tends to zero, the e.m.f. of hydrogen in the metal cannot be $-\infty$ even though Nernst's law predicts so. Other reactions have to be involved.)

The diffusion coefficient of Pd can be calculated both from the time delay (i.e. Δt in fig.1.2) or, more accurately, by fitting the transient. The fit involves two parameters, as shown in Chapter 3. One is the diffusion coefficient D, and the other c^1 is the ratio of hydrogen charge in the pulse to the total hydrogen already present in the sample. In principle, the latter parameter should be determined from experiment ($I \times \Delta t$), but because of diffusion loss through the side of the sample, the oxidation loss (important at small hydrogen concentrations) and the possible loss by formation of bubbles, some adjustment of this parameter is necessary. Table 4.1 gives the experimental values and fitting results of this parameter at various hydrogen concentrations. It can be seen

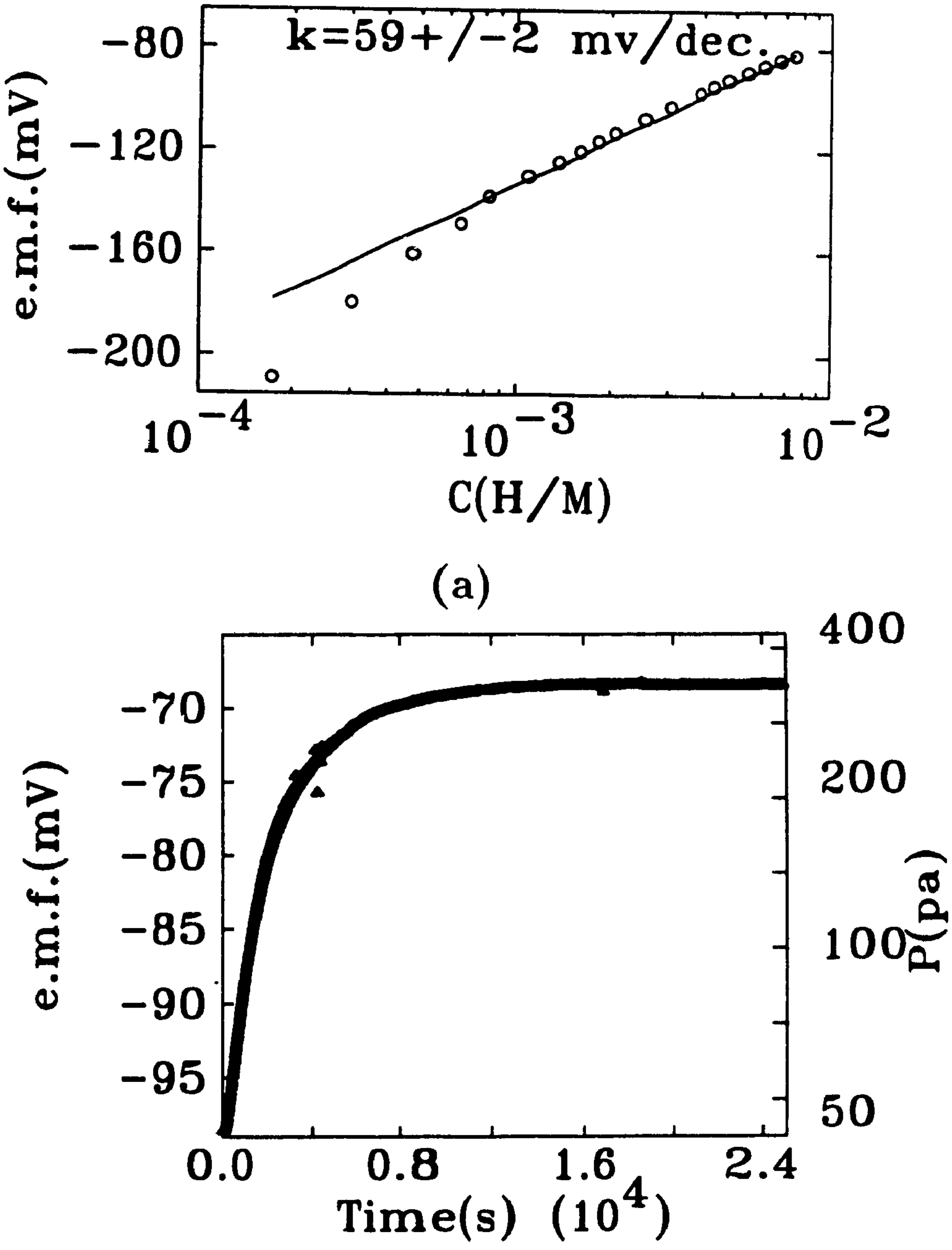

(b)

Figure 4.3: E.m.f. vs. hydrogen concentration for Pd, (a) The equilibrium emf obtained by current pulse technique (b) The emf at the exit side when charging at the entry side with current density of 0.1 $mAcm^{-2}$

$c_0(10^{-3})$	$c^1_{exp}(\%)$	$c^1_{fit}(\%)$	$D(10^{-11}m^2/s)$
2.5	18.8	21.16	4.65±0.03
3.04	16.1	17.7	4.62±0.03
3.88	23.6	20.5	4.28±0.02
4.3	9.8	10.4	4.23±0.04
4.8	9.7	10.1	4.17±0.03
5.4	12.0	12.2	3.95±0.02
6.0	9.9	9.5	3.62±0.03
6.73	10.1	9.6	3.75±0.03
7.5	10.5	8.0	3.75±0.03

Table 4.1: Fitting parameters in current pulse technique for Pd- c^1_{exp} is the experimental value of the ratio, c^1_{fit} the value of fitting results, the error of these parameters is generally a few percent

that generally c^1_{exp} is a few percent different from c^1_{fit}. This agrees with the rough calculation given above. However, in three cases, c^1_{exp} and c^1_{fit} have large differences. At low hydrogen concentrations, this may be caused by other reactions (there is also derivations from linearity in fig.4.3a at these concentrations). The one at higher hydrogen concentrations is a exception which may be an experimental error. The error bars in Table 4.1 is the fitting uncertainty.

Diffusion data are shown in fig.4.4. Clearly D is almost independent of hydrogen

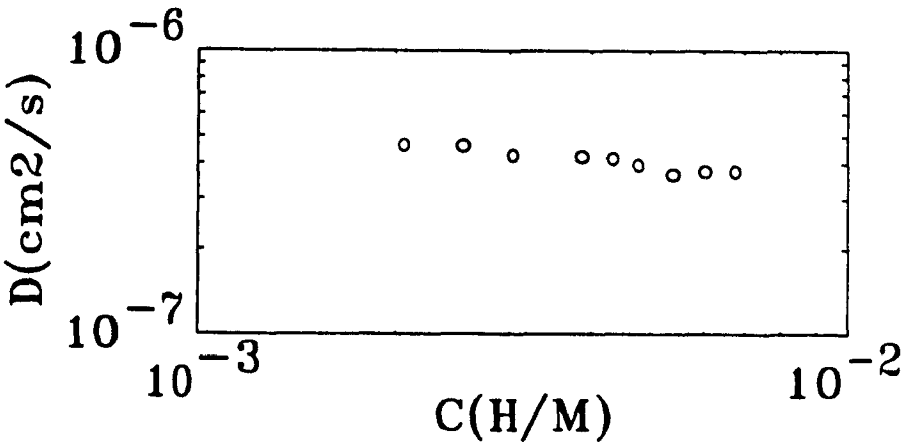

Figure 4.4: Diffusion coefficient of hydrogen in Pd at various hydrogen concentrations

$D(10^{-11}m^2/s)$	3.8	4.0 ± 0.2	3.7	1.3	6.3	3.8	3.2	1.9 ± 0.4
references	[7]	*this work*[1]	[49]	[27]	[3]	[5]	[6]	*this work*[2]

Table 4.2: Comparison of D; *this work*[1]-by current pulse method, *this work*[2]-by potentiostatic method

concentration. In Table 4.2 we shows our results compared with others, agreement with recent work is good.

4.1.2 Potentiostatic method

The last column of Table 4.2 is the results of the potentiostatic method, using a 1M acetic acid solution. The experimental procedure is as follows. The sample is treated in the same way as in the pulse method. The electrolyte is prepared by mixing acetic acid with distilled water. Instead of measuring the e.m.f. at the two sides of the sample, this method measures the current at the two sides of the cell. Initially both sides of the sample are kept at a selected and constant voltage so that no current($< 0.02\mu A$) flows in the cell. This choice makes the surface of the sample, in principle, free of hydrogen. At voltage of Pd 148 mV lower than SCE at exit side and 157 mV lower than SCE at entry side in present electrolyte, the above condition is satisfied (note, there is about 9 mV difference which may arised from the surface contamination we mentioned before). When the cell becomes stable, the potential of the entry side is switched to 196 mV which makes the potential of Pd more negative than the hydrogen-free potential, and thus causes hydrogen to enter Pd. The potential of the exit side is kept constant. After the sudden switch, the current at the entry side increases abruptly and then decays to a constant value, while at the exit side, it remained zero for a well-defined time, then increases slowly and finally reaches a constant value. When current of both sides is constant, the voltage of the entry side is switched to a new value of 248 mV, which causes a larger hydrogen flux into Pd. The process is repeated with V_c increasing 50 mV at each step up to 670 mv. Fig.4.5b shows the relation between V_c and $c(H/M)$. $c(H/M)$ is the concentration of hydrogen in the sample which can be obtained from I_d^{∞}, as described in Chapter 3 (here, V_c is not proportional to lnc because here is not a equilibrium case).

A typical transient of this method is shown in fig.4.5a Because the potential of the exit side is kept constant, every increase of potential at entry side increases the density gradient of hydrogen and hence the current. But problems arise when the content of hydrogen is high, because the current through Pd increases as the H content increases. If the potential between SCE and the sample at exit side is kept constant, the real voltage will drop because of resistivity between SCE and the sample, and not be

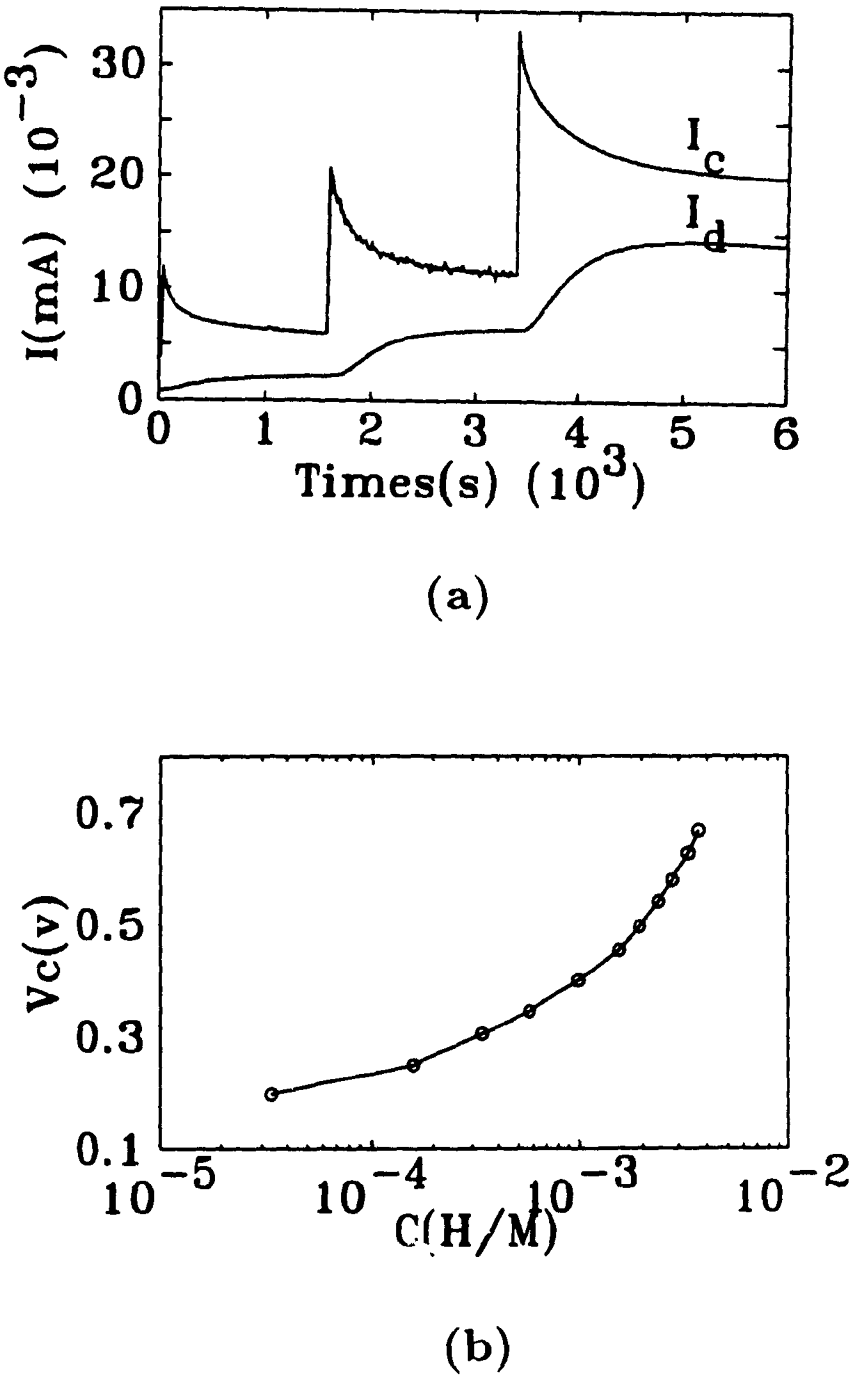

Figure 4.5: (a) Typical transients for Pd in potentiostatic method (b) Hydrogen concentration Vs charging voltage relations

enough to keep the exit side free of hydrogen so that the density gradient of hydrogen will decrease. This is why the current of at the exit side decreases after saturation. This effect is shown in fig.4.5a. To eliminate such an effect, a conventional way is to choose a larger voltage across Pd and SCE at the exit side. However, it takes so long a time for the current at the exit side to become zero that contamination could occur.

The hydrogen concentration was calculated from e.q. (3.33) assuming the gradient is uniform, which is reasonable if the diffusion coefficient does not change with hydrogen concentration. It can be noted from fig.4.5a that ΔI_c^∞ is about twice as large as ΔI_d^∞. The difference between the input and output amount of hydrogen should be the amount of hydrogen inside the Pd. The result is in rough agreement with the value calculated from e.q.(3.33).

The fitting involves two parameters I_∞ and D. They are shown in Table 4.3. It can be seen that D is smaller than the value found from the pulse technique. There are two possible reasons:

1. Surface contamination. After the experiment, it was seen that the entry side of sample was highly contaminated. The surface became black and changed to yellow after a few days of exposure to air. This unknown contaminant reduced the exchange rate of hydrogen at the surface, and hence the apparent diffusion coefficient.

2. The voltage chosen at the exit side. As stated above, when the H content is increased the gradient may drop, which reduces the current, which gives a smaller apparent value of D.

However, this measurement still makes sense and is also consistent with others

$c(10^{-4})$	$\Delta I_{\infty}(\mu A)$	$D(10^{-11}m^2/s)$
0.33	1.24	2.3±0.1
1.58	4.21	2.1±0.1
3.33	7.41	2.6±0.1
5.71	7.21	1.9±0.1
9.87	12.07	1.8±0.1
15.33	14.26	1.6±0.1
19.33	11.94	1.9±0.3
23.97	14.44	1.9±0.3
28.12	12.80	1.9±0.4
33.03	14.49	1.8±0.3
36.67	11.07	1.9±0.8

Table 4.3: Fitting parameters in potentiostatic method for Pd

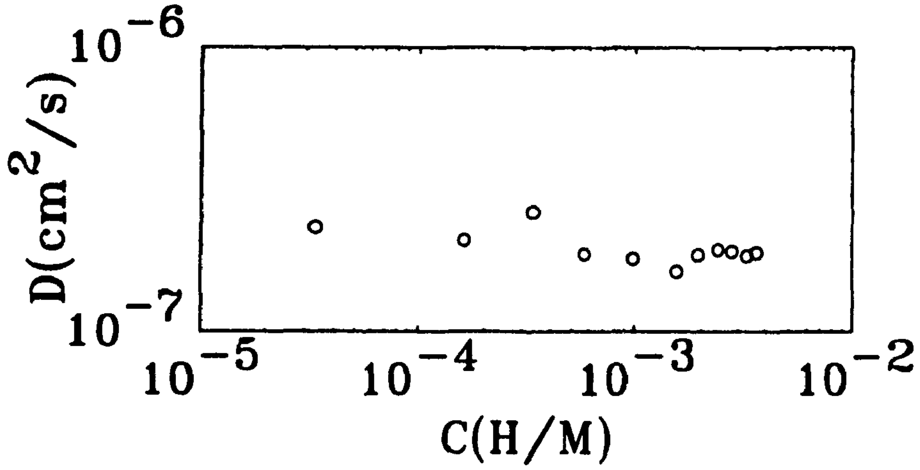

Figure 4.6: Diffusion coefficient of H in Pd obtained from potentiostatic method

results to some extent. Fig.4.6 shows D at different hydrogen concentration. It is easy to see that D does not change significantly with hydrogen concentration. Actually, it is essential that D be constant over a wide range of hydrogen concentration for this method to be workable, because a large H concentration gradient is essential to get current through the sample.

4.2 $Ni_{60}Zr_{40} - H$ system

After X-ray examination (amorphous $Ni_{60}Zr_{40}$), the sample was mounted on the cell directly. No cleaning was necessary because the sample comes straight from high vacuum and is not significantly contaminated during the X-ray process. The surface with the thin layer of Pd was used as the exit side; the other surface was used as the entry side.

4.2.1 Potentiostatic method

Initially, we used the potentiostatic method to study hydrogen diffusion. The electrolyte was 1M acetic acid. When both sides of the cell becomes stable(the potential of the sample is typically 200 mV lower then the reference electrodes), the potential of the charge side is changed to 600 mV to charge the sample with hydrogen. The transient at exit side is shown in fig.4.7.

Above the noise (created maybe by fluctuations in the power supply net work), I_d increases with time, but in a way qualitative different from Pd. We believe this is be-

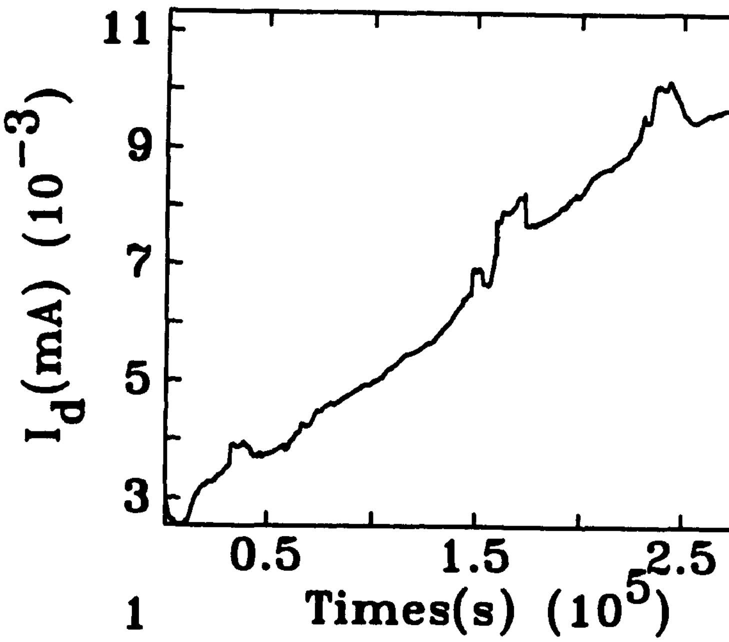

Figure 4.7: Potentiostatic transient for Ni-Zr

cause the diffusion coefficient of hydrogen varies strongly with hydrogen concentration. This dependence makes it virtually impossible to analyze the data of fig.4.7. However, we can estimate D from the fact that after the entry side has been switched to a new voltage, nothing is seen at the exit side until about three hours later. Using this time delay to estimate D(with $25\mu m$ in thickness, and using $D \sim \frac{l^2}{t_0}$, where t_0 is the time delay) , we obtain $D \sim 6 \times 10^{-14} m^2/s$ (the error of this value can be 100%).

4.2.2 Current pulse method

After the sample is mounted in the cell, it takes typically a few hours for the cell to stablize. The cell was kept at rest condition for 15 hours before the first charging pulse was applied (the change of e.m.f. at exit side after this long period was less than 0.05 mV in 30 minutes).

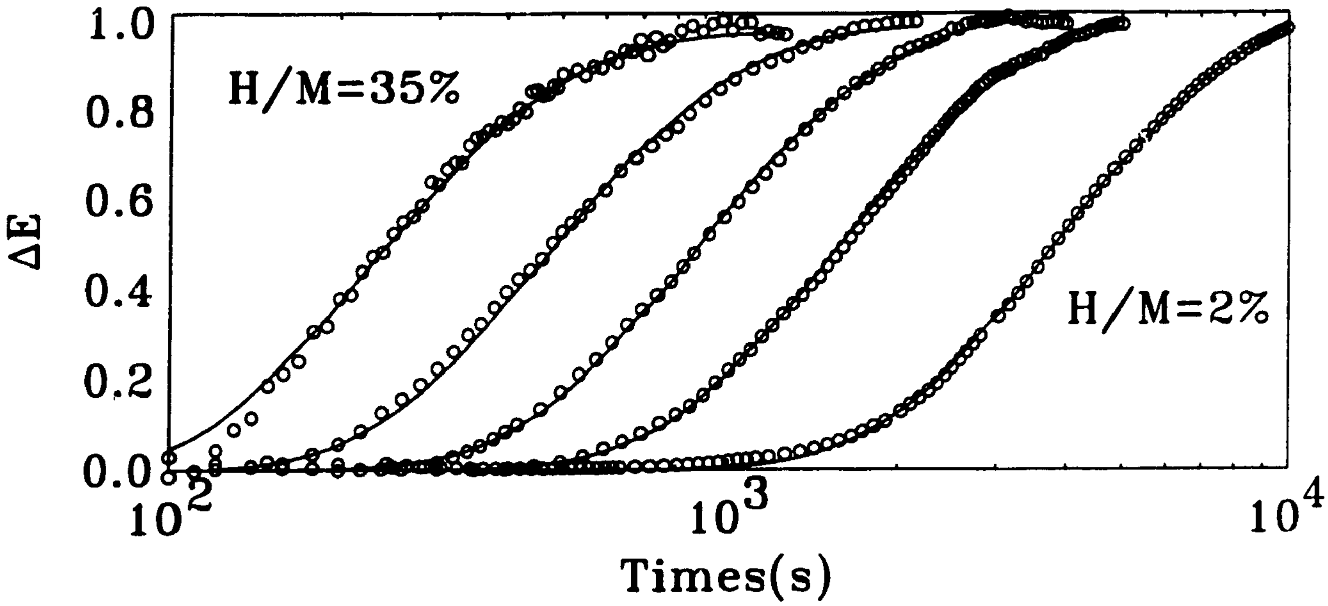

Figure 4.8: Typical transient for Ni-Zr by current pulse technique

The typical transient at the entry and exit side is shown in fig.4.8. Two points should be noted:

1. As was the case for Pd, there is a potential difference between the entry side and exit side, but now the situation is more complicated. The side with Pd (exit side) is very stable, and the changes in e.m.f. with time are smooth and continuous after a pulse is applied at the entry side. This is similar to the case of Pd. But the side without Pd (entry side) is much more complicated. After the first few pulses, the e.m.f. changes smoothly at the beginning and seems to be predictable. But at later times (over 1 hr) the behavior becomes irregular, and the sudden changes of e.m.f. changing tendency sometimes can be seen. After a few pulses, the behavior becomes smooth and regular (or predictable).

2. When the hydrogen concentration is low, the equilibrium e.m.f. of the entry side is smaller than at the exit side. However, as the hydrogen content is raised, the difference becomes smaller, and finally the two cross over, so that the e.m.f. at the exit side become larger than at the exit side. This is quite different from the behavior in Pd.

The equilibrium potential differences between the entry side and exit side, probably results from the two surfaces being different materials (exit side is Pd, entry side is $a - Ni - Zr$ or ZrO_2). Complete understanding of this phenomena will needs a careful study of the interface between the sample and the electrolyte (band structure etc.). However, there are few such studies even for crystalline materials.

When the sample was loaded with hydrogen, it expands significantly. A cap -like expansion was formed on the sample at the charging area. This expansion ceased after the sample was unloaded from the cell for a few weeks (because the hydrogen escapes).

The emf of H in $Ni_{60}Zr_{40}$

The emf of the exit side at various hydrogen concentrations are shown in fig.4.9. Two points can be noted from this diagram.

(1) There is no plateau, which is usually seen in the p-c isotherms of crystalline metal hydrides and corresponds to a phase transition, even when the hydrogen concentration has reached 35% in H/M. This agrees with previous results[17, 9, 32].

(2) The slope of fig.4.9 is 117 ± 2 mv/decade, implying that theoretical (Sievert's law) value of 59 mv/decade ($\frac{RT}{F} ln10$) in Chapter 3 is not valid in the present case.

Because Sievert's law implied that the hydrogen concentration is proportional to the square root of the hydrogen pressure applied to the metal, the slope of 117 mv/decade implies that the hydrogen concentration in amorphous $Ni_{60}Zr_{40}$ is proportional to the fourth root of hydrogen pressure (assuming that hydrogen at these pressures can be treated as an ideal gas). Similar results are found by Spit et al. using gas loading in a amorphous $Ni - Zr$ sample[9].

As mentioned in Chapter 2, the p-c isotherms of amorphous metal hydrides can be described by assuming that sites for hydrogen atoms in the amorphous metal have different binding energies[8, 32]. In $Ni - Zr$, there are several kinds of site (4Zr, 3Zr-1Ni, and 2Zr-2Ni). The spectrum of energies for each kind of site, can thought to be continuous and corresponding densities of sites n has been given as a Gaussian function by Harris[32] and Kirchheim[8]

$$n(E) = \frac{dN}{dE} = \frac{1}{\sigma\sqrt{\pi}} exp[-(\frac{E - E^0}{\sigma})^2] \tag{4.1}$$

where dN is the number of sites available for hydrogen at energy E within the interval dE, E^0 is the mean energy related to a standard state and σ is the width of the Gaussian function. Fermi-Dirac statistics have to be applied to obtain the occupancy because hydrogen atoms exist in the metal as proton

$$o(E) = \frac{n(E)}{1 + exp(\frac{E-\mu}{RT})} \tag{4.2}$$

where μ is the Fermi energy of hydrogen or its chemical potential. The total number of hydrogen atoms or its concentration is obtained by integration of last equation

$$c = \int_{-\infty}^{\infty} o(E) dE \tag{4.3}$$

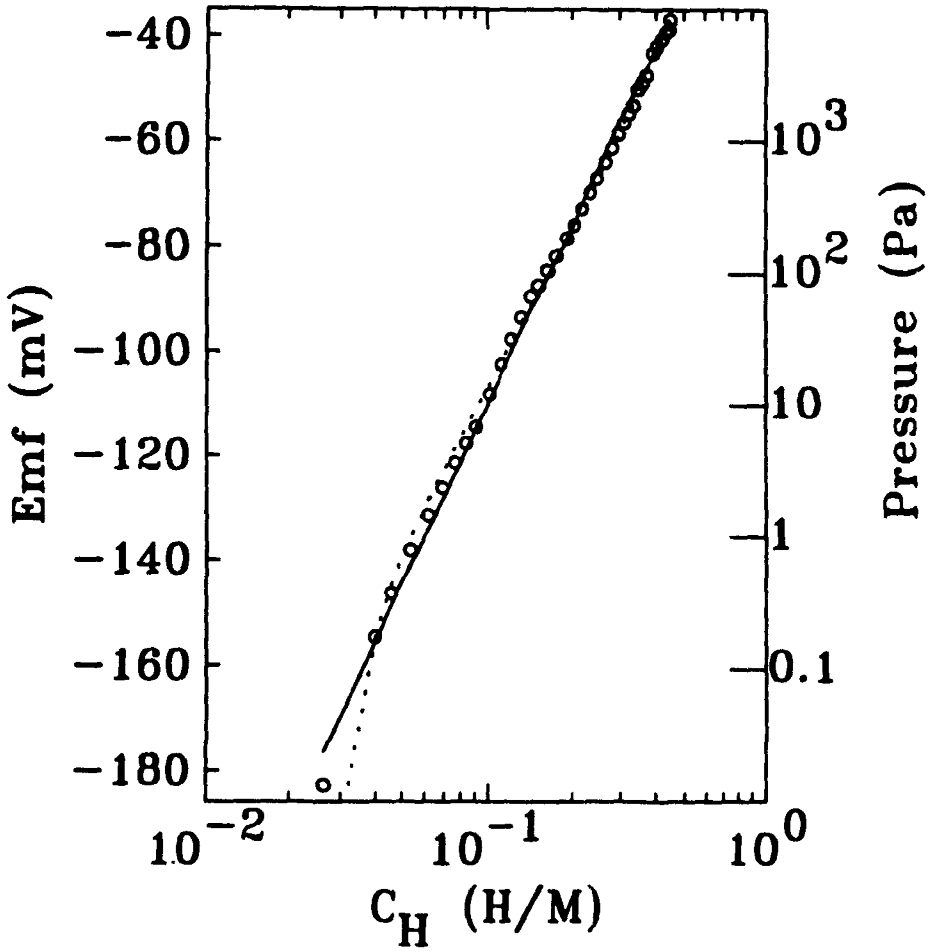

Figure 4.9: E.m.f. Vs. hydrogen Concentrations in Ni-Zr, solid straight line has slope of 117±2 mV/decade, dotted line is the fitting results according to eq.(4.5) with $E^0 = -21.4mv$, $\sigma = 79mv$, and $c_0 = 3.6\%$.

If the Fermi-Dirac function is approximated by a step function ($\mu \gg RT$), we can ignore the high order terms of the above integral, we get

$$2c = 1 + erf(\frac{\mu - E^0}{\sigma}) \tag{4.4}$$

We tried to fit our experimental result with this formula. with the two parameters E^0 and σ. However, deviations arise at low hydrogen concentrations, because the above treatment is too simplified. We already know that in amorphous $Ni - Zr$ several kinds of sites are available for hydrogen. The lowest energy site, surrounded by 4-Zr atoms, is definitely so low[32, 17] (lower than the e.m.f. region we can measure using electrochemical method because of oxidation etc.) that the hydrogen in these sites cannot diffuse out, once filled. To see if a gaussian distribution for the higher energy sites (e.g. 3Zr-1Ni site) can explain the emf behavior, we therefore have to subtract these low energy sites from the measured total hydrogen concentrations. Assuming the Zr_4 sites are simply filled and hydrogen in these sites does not diffuse, another fitting parameter will involve in eq.(4.4) which becomes

$$2(c - c_0) = 1 + erf(\frac{\mu - E^0}{\sigma}) \tag{4.5}$$

Where c_0 is the total number of occupied Zr_4 sites. A good fit was obtained using eq.(4.5) (also shown in fig.4.9). The parameters we got are: $E^0 = -21.4$ mv, $\sigma = 79$ mv, $c_0 = 3.6\%$. E^0 and σ value are consistent with the results of Kirchheim et al.[8] The width also agrees with the computer generated results of Batalla et al. [17]. Since in amorphous metals, different kinds of metal atom are distributed randomly, the possibility that a H atom is surrounded by 4 Zr atom will be proportional to x^4, with

x the composition of Zr in $Ni_{1-x}Zr_x$. Similarly, the possibility that H is surrounded by 3 Zr and 1 Ni atoms will propotional to $x^3(1-x)$, etc. Harris et al. [32] suggested that there is a common coefficient in this proportioning (1.9 for melt-spun materials). Using this number to calculate the total number of 4Zr site, we obtain 1.8% which is close to our c_0 value. Also, if we extend our pressure region to the region of Batalla's(equivalent to an e.m.f. of +30 mv), the total hydrogen concentration extrapolates to 80% H/M. This value is in perfect agreement with the results of Batalla et al. [17] for similar alloy composition (see fig.4.10 for the filling of this gaussian distribution). Comparing our emf value to the binding energy of hydrogen in reference[17], we can conclude that hydrogen will mainly occupy Zr_3Ni tetrahedral sites. This conclusion is not inconsistent with neutron scattering experiment by Suzuki et al.[14] and Batalla et al.[17].

Diffusion behavior of hydrogen in $Ni_{60}Zr_{40}$

As we said earlier, surface conditions do not influence the diffusion coefficient derived from current pulse technique very much[49], provided they do not entirely prevent penetration of hydrogen into the and escape of hydrogen out of the sample. It is only necessary to produce, at the entry side of the sample, a concentration peak sufficient to obtain a detectable signal at the exit side. Therefore, even though there maybe a potential difference between the entry side and exit side when the emf at exit side saturates, our results for diffusion are not affected.

Fitting to get the diffusion coefficient through e.q.(3.33) here is a little bit different

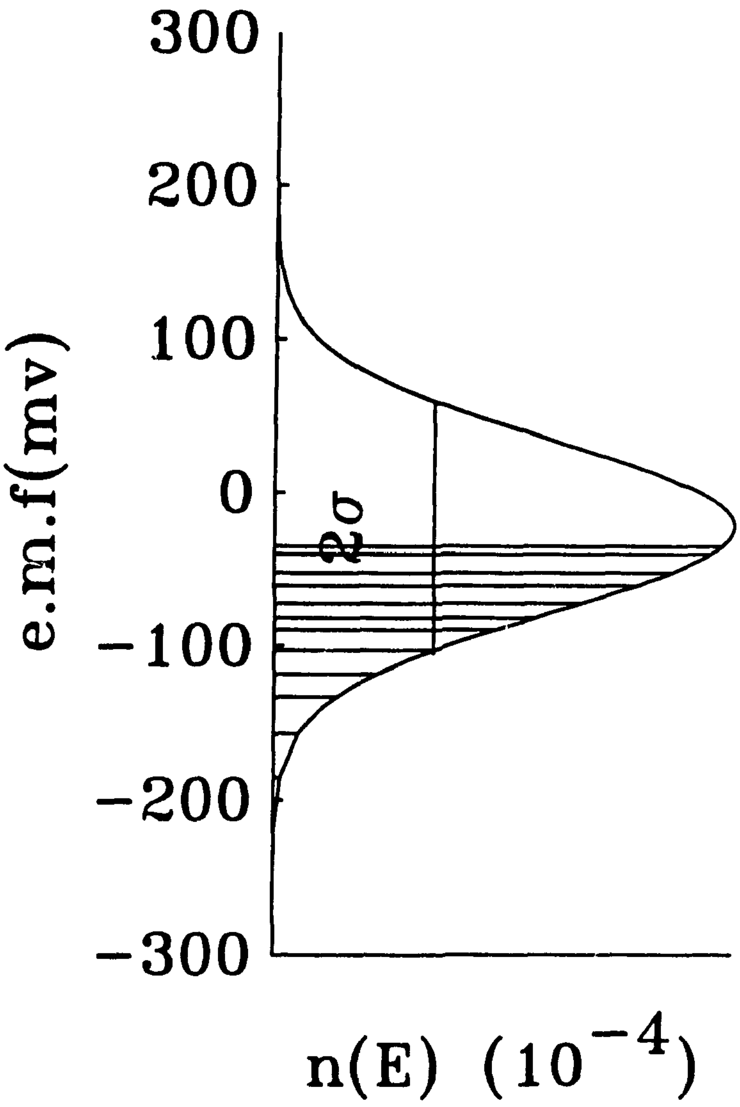

Figure 4.10: The filling of the sites

$c_0(10^{-2})$	c^1_{exp}	c^1_{fit}	$D(10^{-14}m^2/s)$		$c_0(10^{-2})$	c^1_{exp}	c^1_{fit}	$D(10^{-14}m^2/s)$
3.99	0.5475	0.5838	2 37±0 02		17 64	0.0863	0.0841	15 18±0 03
5.38	0.1533	0.1536	3.19±0.01		19 15	0.0616	0.0590	16 71±0 06
6.18	0.1228	0.1238	3.76±0 02		20.32	0.0778	0.0750	17.70±0.05
7.65	0.0980	0.1028	5.17±0.03		21.89	0.0677	0.0658	19 32±0 09
8.39	0.0899	0.0909	4.80±0.02		23.36	0.0631	0 0620	20.71±0 12
9.13	0.1218	0.1469	5.79±0.02		24 82	0.0747	0 0641	21 18±0 16
10.22	0.1095	0.1327	6.81±0.02		26 66	0.0616	0.0560	25 17±0 19
11.32	0.0979	0.1143	7.79±0.02		28.30	0.0520	0.0523	24.0±0 31
12.42	0.0894	0.1003	9.19±0.02		29.76	0.0444	0.0491	26 89±0.17
13.51	0.0819	0.0937	10.46±0.02		31.08	0.0377	0.0324	31 09±0.19
14.61	0.0571	0.0565	11 88±0.06		32 24	0.0366	0.0281	34 27±0 18
15.43	0.0721	0 0726	12.68±0.04		34.59	0.0319	0 0247	39.51±0 27
16.54	0.0670	0.0695	13.59±0.04					

Table 4.4: Fitting parameters in Ni-Zr-H system

from Pd, since the slope of e.m.f-log H/M in Ni-Zr-H is different from in Pd. We have to use the experimental value.

The fitting also involves two parameters D and c_1. Similar to Table 4.1, fitting parameters are listed in Table 4.4

The first and fourth column of Table 4.4 is the concentration of hydrogen(H/M). It can be seen that the difference between theory and experiment is usually small.

large differences only appearing at hydrogen concentrations of around 10% and 30% H/M. This appears as the deviation from the general trend on the D-H/M diagram, a kink on D-H/M diagram (see fig.4 11). In fact, Kirchheim et al reported a a similar kink at D-H/M diagram at a hydrogen concentration of about 35% H/M They interpreted this kink as a transition of the filling of hydrogen sites from 3Zr-1Ni to 2Zr-2Ni sites. In our case, however, the "kink" usually arises when large deviation of c_{fit} from c_{exp} exist. Therefore, we do not believe that the "kink" represents a site-filling transition from 3Zr-1Ni to 2Zr-2Ni, but a experimental artifact.

In fig.4.11, it is also easy to see that D is highly dependent on hydrogen concentrations (it increases twenty times as the hydrogen concentration increases from 4% to 34%). However, since the change of the hydrogen concentration is very small at every step (typically 1 to 2 percent H/M) we ignored the change of diffusion coefficient (about $1 \times 10^{-14} m^2/s$) in our fitting. In fact, this approximation is reasonable, as is shown by the fit and the consistency of most experimental measured c^1 with fitted c^1.

The charging step cannot be too large , otherwise, no meaningful value of D may be found. Furthermore, the initial conditions for the current pulse are not valid any more. This is because when the hydrogen concentration is high, hydrogen diffuses fast and thus it takes a short time for the hydrogen to diffuse through the sample; however, since $E \sim ln(H/M)$, it needs large amount of charge in a current pulse (i.e. large current (5 to 10 mA) times long time (30 seconds)) to create a measurable emf change, and this will break the boundary conditions (because the charging time is comparable with the diffusion time (about 100 seconds)). Therefore, the diffusion measurement at

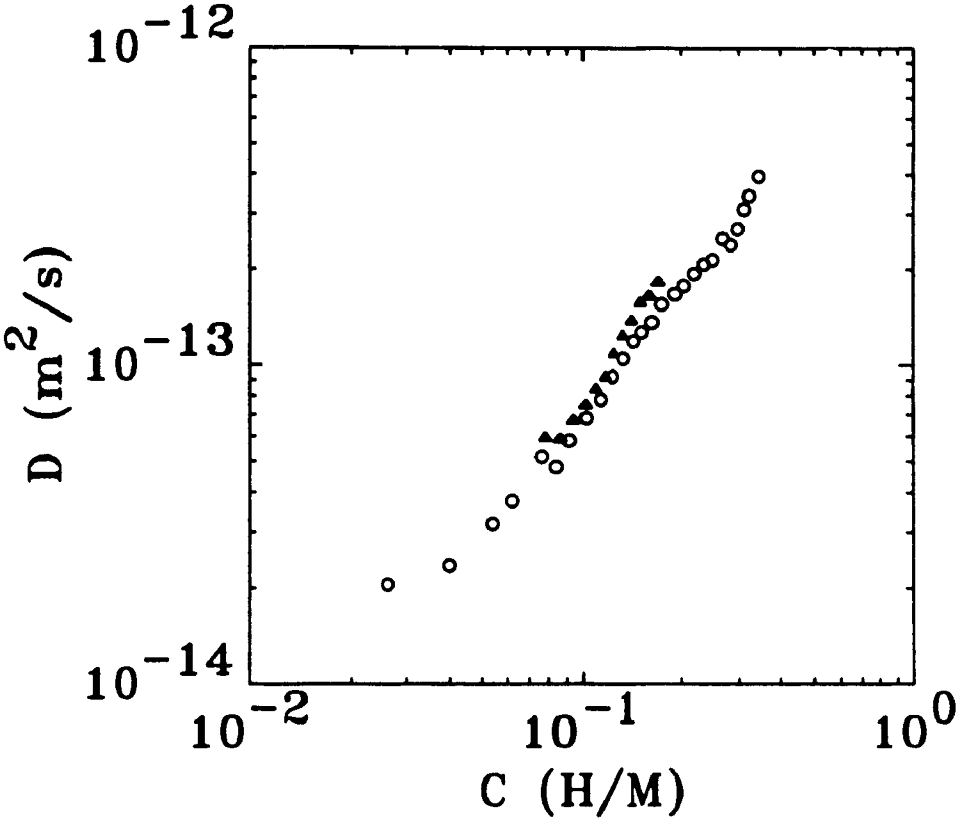

Figure 4.11: Diffusion Coefficient of hydrogen in Ni-Zr at various hydrogen concentrations for two samples

high hydrogen concentrations is not reliable and can only be used for a rough estimate of the diffusion constant.

As has been mentioned in Chapter 2, the explanation of the diffusion behavior of hydrogen in amorphous metals is not easy. Actually, it is still not clear what is the mechanism of hydrogen diffusion even in crystalline materials[3]

The simplest model to describe the hydrogen diffusion behavior is by assuming the diffusion process is random walk with thermally activated jump from one interstitial site to another.

With regard to amorphous alloys, Kirchheim et al.[8] simplified the diffusion process assuming a continuous distribution of sites with continuous distribution of energy. With some approximations (all sites have the same saddle point energy, every jump process have the same mean jump distance, blocking factor is one, etc), Kirchheim et al. got the following expression for diffusion coefficient:

$$D_{ef} = D\frac{\partial}{\partial c}(1-c)^2 exp(\frac{\mu - E_0}{RT}) \tag{4.6}$$

or, for low hydrogen concentrations

$$D_{ef} = \frac{D}{RT}\frac{\partial \mu}{\partial c} exp(\frac{\mu - E_0}{RT}) \tag{4.7}$$

Where $D = D_0 exp(-Q/kT)$ is tracer diffusion coefficient (does not depend on hydrogen concentration) with Q as activation energy and D_0 as diffusion coefficient at 0K, μ is the chemical potential of hydrogen in the metal, E_0 the average binding energy of hydrogen.

Eq.(4.7) was used to fit their results for amorphous $Pd_{77.5}Cu_6Si_{16.5}$ and $Ni_{49.9}Pd_{31.8}P_{18.3}$ at small hydrogen concentrations (less than a few percent).

However, eq.(4.6) predicts that when hydrogen concentration $c = 0.5$, $D = 0$ which is unphysical (R. Griessen et al [39] had a similar disagreement with eq.(4.6)). R.C. Brouwer et al.[39] derived another expression for $Nb_{1-y}V_y$ alloys in 1988[39].

$$D^* = \sum_{ij} \frac{D^0_{ij}}{RT} c_i q_{ij} [1 - \frac{c_j s_j}{p_j}] exp[-E_{ij}(c)/RT] \frac{\partial \mu}{\partial c} \tag{4.8}$$

The coefficients q_{ij} is the probability of finding sites of type j next to sites of type i, p_j is the probability of finding sites of type j in the alloy, c_j the probability of finding an interstitial atom on sites of type j, s_j is the blocking factor of site j, E_{ij} is the activation energy for diffusion from site type i to j, and D^0_{ij} the diffusion constant from i to j at 0K

To apply this theory to amorphous materials, we have to make some approximations. Following Kirchheim et al.[8], we let $q_{ij} = p_j = n(E_j)$, $s_j = 1$, (the first equation means that there is no correlation between site i and j: whatever a site is, the probability of finding site j next to this site is still p_j or $n(E_j)$ in e.q.4.1; the second equation simply means that there is no blocking affect. In fact, c_j in e.q.4.8 is identical to $o(E_j)$ in e.q.4.2). Making the same approximation for activation energy (all sites have a the same saddle point energy $E^0 + Q$, so the activation energy $E_{ij} = E^0 + Q - E_i$), we obtain.

$$D = \frac{D^0}{RT}(1-c)^2\frac{\partial\mu}{\partial c}exp(\frac{\mu - E^0 - Q}{RT}) \qquad (4.9)$$

or

$$lnD = lnD^0 + 2ln(1-c) + ln(\frac{1}{RT}\frac{\partial\mu}{\partial c}) + \frac{\mu - E^0 - Q}{RT} \qquad (4.10)$$

From experiment, we have $\mu = 2RTlnc$ (fig.4.9), so finally

$$lnD = ln2D^0 + 2ln(1-c) - \frac{E^0 + Q}{RT} + lnc \qquad (4.11)$$

This expression eliminates the problem of $D = 0$ when $c = 0.5$. Therefore the concentration dependence of diffusion coefficient will be

$$D = 2D(T)c(1-c)^2 \qquad (4.12)$$

where $D(T) = D^0exp(-\frac{G^0+Q}{RT})$ does not depend on hydrogen concentration

Eq.(4.11), however, does not reproduce the experimental data as can be seen in fig.4.12. Therefore, there must be some additional physical processes in eq.(4.8).

In fact, at high hydrogen concentrations, the approximations we made before may not valid. The correlation factor q_{ij} cannot be simply treated as p_j. When a site has been occupied, the nearest site is not available (exclusion effect)[17] for the next hydrogen. This factor also has to be considered.

The simplest way to include the correlation factor is to assume the concentration dependence is linear $1 + Ac$. Then

$$D = 2D(T)(1 + Ac)c(1 - c)^2 \tag{4.13}$$

Fitting the experiment data with this formula, we got $2D(T) = 3.86 \pm 0.37 \times 10^{-9} cm^2/s$ and $A = 12.4 \pm 0.5$. This means that when hydrogen concentration reached about 10%, the correlation contribution is about the same order as that of random walk. So only when hydrogen concentration is lower than 0.8% , can we ignore the effect of correlations in the error of about 10 percent. Thus when hydrogen concentration reaches about one percent, they can affect each other. Assuming a cubic block for hydrogen atoms, the size of this cubic will corresponds to 2.2 metal atomic spaces. Therefore, the distance between hydrogen atoms will be about 0.35 nm (choosing the metal atom size as 0.16 nm (Zr)). The fitted results are shown in fig.4.12. In fact, when hydrogen concentration is high, the situation is very complicated. The reason why the correlation factor might linearly depend on the hydrogen concentration is not clear. Furthermore, even if the relation is reasonable, whether it can be used to other

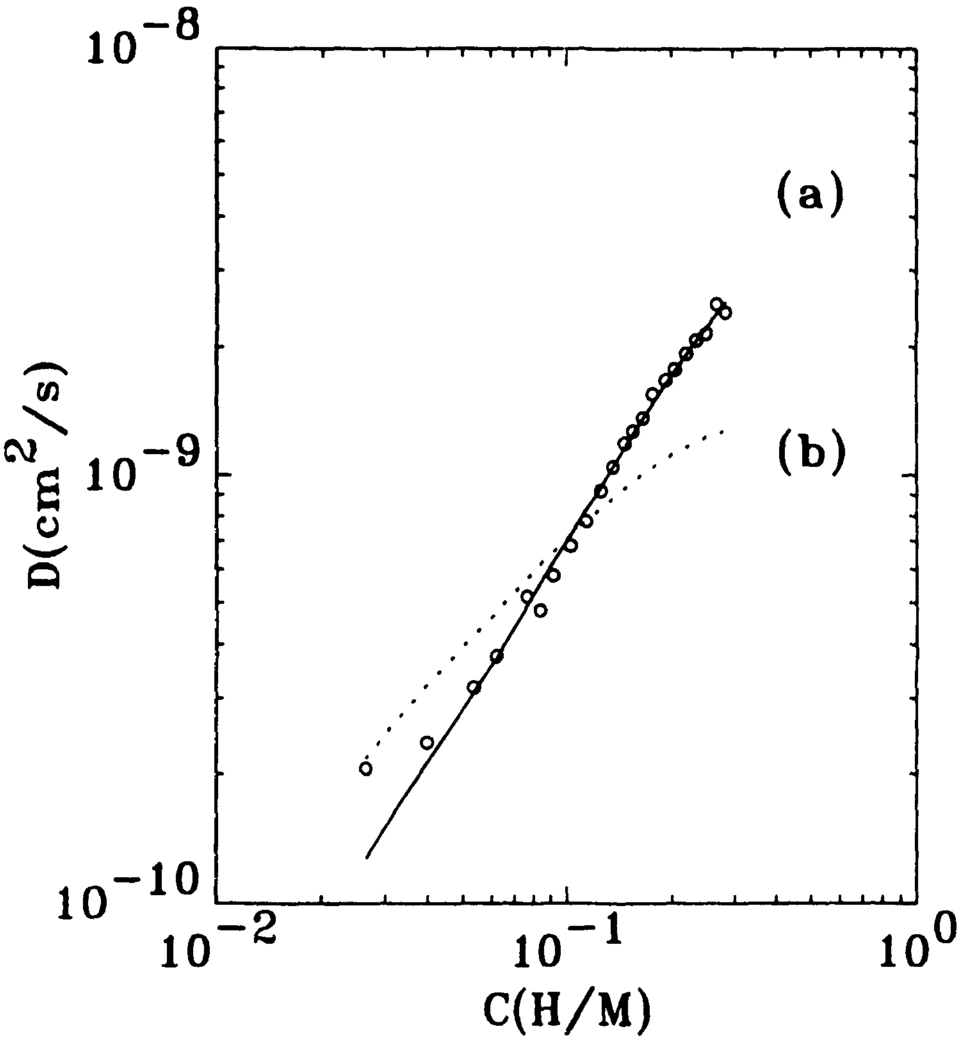

Figure 4.12: The fitting of the diffusion constant (a) solid line: $D = 2D(T)(1 + Ac)c(1 - c)^2$, $2D(T) = 3.86 \pm 0.37 \times 10^{-13} m^2 s^{-1}$, $A = 12.4 \pm 0.5$; (b) dotted line: $D = Ac(1 - c)^2$, $A = 8.74 \pm 0.54 \times 10^{-13} m^2 s^{-1}$

systems is not clear either. Obviously, more work is needed.

Chapter 5

Conclusions

The current-pulse technique has proved to be an effective method for studying hydrogen diffusion and storage in amorphous alloys.

The results shows that in $Ni_{60}Zr_{40}$, the diffusion coefficient of hydrogen increased more than one decade with concentration increasing between 4% and 30% H/M. The explanation of diffusion coefficients need a linear concentration dependence of correlation factor in addition to the gaussian distribution of hydrogen binding energy. Why it should be so is still not clear. More theoretical work is needed.

The results of chemical potential of $H - Ni_{60}Zr_{40}$ is different from the crystalline metal hydrides. The concentration dependence of emf shows that the Sievert's law is not valid for $H - Ni_{60}Zr_{40}$ at any hydrogen concentration. A gaussian distribution of hydrogen binding energy can be used to explain the emf behavior.

Although the application of the current-pulse method is successful here, there is also limitation. Apart from the increasing of surface contamination, the e.m.f. and temperature region are limited in this method. Furthermore, we need the temperature dependence of diffusion coefficient to derive the activation energy of hydrogen diffusion. The interface behavior is not understood either.

Immersing our cell in a thermal bath, we would be able to study the diffusion behavior at different temperatures. With at least two sources in sputtering system, we would be able to keep our sample fabrication in high vacuum, therefore, eliminate the effect of ZrO_2. These will be our next projects.

Bibliography

[1] T. Graham, Phil. Trans. Roy. Soc. (London) **156** (1866) 399

[2] e.g. B. Hjorvarsson and J. Ryden in Int. Sym. on Metal-Hydrogen systems (Banff, Alberta, Canada sept. 2-7,) 1990, P45

[3] "Hydrogen in Metals I", Vol. 28 of Topics in Applied Physics, edited by G Alefeld and J.Vokl, Chapter 2 by H. Wagner

[4] Kangjo Cho et al., J. Less-Common Metals, **89** (1983) 223-228

[5] e.g. "Hydrogen Entry and Action in Metals" by M.A. Fullenwider . Pergamon Press (New York 1983)

[6] B.S. Berry, Scripta Metall., **16** (1982) 1407

[7] R.Kirchheim and R.B. McLellan, J. Electrochem. Soc. **127** (1980) 2419

[8] R. Kirchheim, F. Sommer and G. Schluckebier, Acta Metall. **30** (1982) 1059

[9] F.H.M. Spit, J.W. Drijver, W.C. Turkenburg and S. Radelar, Journal de Physique **41** (1980) C8-890

[10] A.J. Maeland, L.E. Tanner and G G. Libowitz, J. Less-Comm. Met. **74** (1980) 279

[11] J.J. Rush, J.M. Rowe and A.J Mealand, J. Phys. **F10** (1980) L283

[12] H. Kaneko, T. Kajitani, M. Hirabayashi, M. Ueno and K. Suzuki, Proc. 4th Int. Conf. on Rapidly Quenched Metals , Sendai, Japan (1981) vol.2 1605

[13] K. Kai, T. Fukunaga, T. Nomoto, N. Watanabe and K. Suzuki, Proc. 4th Int. Conf. on Rapidly Quenched Metals, Sendai, Japan (1981) vol.2 1609

[14] K. Suzuki, K. Hayashi, Y. Tomizaka, T. Fukunanga and K. Kai, J. Non-Cryst. Solids **61** (1984) 637

[15] K. Samwer and W. Johnson, Phys. Rev. **B28** (1983) 2907

[16] S.M. Fries, H.G. Wagner, S.J. Campbell, U. Gonser, N. Blaes and P. Steiner, J Phys. **F15** (1985) 1179

[17] E. Batalla, J.O. Strom-Olsen, Z. Altounian, D. Boothroyd and R. Harris, J. Mater. Res. **1** (1986) 765

[18] L.J. Lewis and R. Harris, J. Phys. **F13** (1983) 1359

[19] C.H. Bennett, J. Appl. Phys. **43** (1972) 2727

[20] (a) K. Aoki, M. Kamachi, and T. Masumoto J. Non-Cryst. Solids **61** & **62** (1984) 679 (b) K. Aoki, A. Horata and T. Masumoto in Proc. of 4th Int. Conf. on Rapidly Quenched Metals, Sendai, Japan (1981) vol.2 1649

[21] F.H.M. Spit, J.W. Drijver, and S. Radelar, Z. Physik. Chemie NF **116** (1979) 225

[22] C.H. Hwang. S. Kang, K. Cho and K. Kawamura, Scr. Metall. **20** (1986) 1231

[23] K. Dini and R.A. Dunlap, J. Phys. **F15** (1985) 273

[24] A.J. Mealand in "Hydrogen in disordered and amorphous solids" edited by G. Bambakidis and R.C. Bowman (Plenum, New York, 1986) P127

[25] e.g. B. Rodmacq, M. Maret, J. Laugier, L. Billard and A. Chambarod, Phys. Rev. **B38** (1988) 1105

[26] U. Stolz, M. Weller and R. Kirchheim Scr. Metall. **60** (1986) 1361

[27] J. McBreen, L. Nanis, W. Beck, J. Electrochem. Soc. **113** (1966) 1218

[28] R. Kirchheim, T. Mutschele and W. Kieninger, Proc. 6th Int. Conf. on Rapidly Quenched Metals , canada, vol.3 (1988) 457

[29] A. Szokefalvi-Nagy, S. Filipek and R. Kirchheim, J. Phys. Chem. Solids **48** no.7 (1987) 613

[30] P.M. Richards, Phys. Rev. **B30** (1984) 5183

[31] U. Stolz, R. Kirchheim, J.E. Sador and M. Laridjani, J. Less-Common Metals. **103** (1984) 81

[32] J.H. Harris, W.A. Curtin and M. Tenhover, Phys. Rev. **B36** (1987) 5784

[33] J.K. Norskov and N.D. Lang, Phys. Rev. **B21** (1980) 2136

[34] B.S. Berry and W.C. Pritchet, Journal de Physique **46** (1985) c10

[35] R.C.Jr. Bowman and A.J. Mealand, Phys. Rev. **B24** (1981) 2328

[36] R.C.Jr. Bowman in "Hydrogen in disordered and amorphous solids" edited by G. Bambakidis and R.C. Bowman (Plenum, New York, 1986) 185

[37] R. Griessen, Phys. Rev. **B27** (1983) 7575

[38] R. Kirchheim and U. Stolz; Acta Metall.**35** (1987) 281

[39] R.C. Brouwer, E. Salomons, and R. Griessen, Phys. Rev. **B38** (1988) 10217

[40] "Physical Chemistry" by Gordon M. Barrow, Fourth edition, Published by McGraw-Hill Inc. (New York 1979) P606

[41] J.T. Markert, E.J. Cotts and R.M. Cotts; Phys. Rev. **B37** (1988) 6446

[42] Y.S. Lee and D.A. Stevenson, J. Non-Cryst. Solids **72** (1985) 249

[43] F.H.M. Spit, J.W. Drijver, W.C. Turkenburg and S. Radelaar, J. Phys. (Paris), Colloq. C8, **41**(1980) 890

[44] "Physical Chemistry" by Gordon M. Barrow, Fourth edition, Published by McGraw-Hill Inc. (New York 1979) P287

[45] Bruning and Sieverts, Z. Physik. Chem. **163A** (1933) 409

[46] U. Koster, H-W Schroeder and M. Blank, J. Non-Crystalline Solids **61&62** (1984) 673-678

[47] Yiming Huai; M.Sc., University of Montreal "Preparation and characterization of sputtered amorphous Ni-Zr films"

[48] D. Khatamian and F.D. Manchester, J. Nuclear Mater. **166** (1989) 300-306

[49] H.Zuchner, Z. Physik. Chemie NF **146** (1985) s217-229

[50] Y. Sakamoto, J. Phys. Chem. of Solids **49** No.8 (1988) p897-903